Lisbon Valley, Utah Gas Processing Plant Monitoring, Reporting, and Verification Plan

UIC Class II well

Table of Contents

1.0 - Introduction

Green Natural Gas (GNG) Energy owns and operates a gas processing plant in the Lisbon Valley of southeastern Utah. Starting in 2015, injection of acid gas (a combination of hydrogen sulfide (H_2S) and carbon dioxide (CO_2)) has been ongoing into the Leadville Formation for the primary purpose of disposal and the secondary purpose of the geologic sequestration of CO_2. The natural gas processed at the plant is sourced from fields other than the Lisbon Field, including Aneth and Three Mile Unit (Figure 1). These fluids are piped to the plant. The Carbon Science Initiative (CSI) at the Energy and Geoscience Institute (EGI) at the University of Utah has assembled this monitoring, reporting, and verification (MRV) plan to allow for the fulfillment of the 40 CFR § 98.440-449 Subpart RR regulations.

2.0 - Project Description

2.1 - Past Work

The CSI team has participated in and led work within the Paradox Basin (Figure 1), including the federally funded Southwest Regional Partnership for Carbon Sequestration (SWP) project (DE-FC26-05NT42591), the Improving Production in the Emerging Paradox Oil Play project (DE-FE0031775), the Polymer Membrane for Direct Air Capture (DAC) project (DE-FE0031968), and a feasibility study of CO_2 capture from flue gas using Amine (CarbonSAFE Project, DE-FE0029280). Additionally, the CSI team is participating in the Arizona State University (ASU) Regional DAC project. This project has not yet commenced, therefore preliminary information about this project cannot be provided at this time. We present a brief description and overview of each project to demonstrate our technical capabilities for developing this MRV plan, especially within the Paradox Basin.

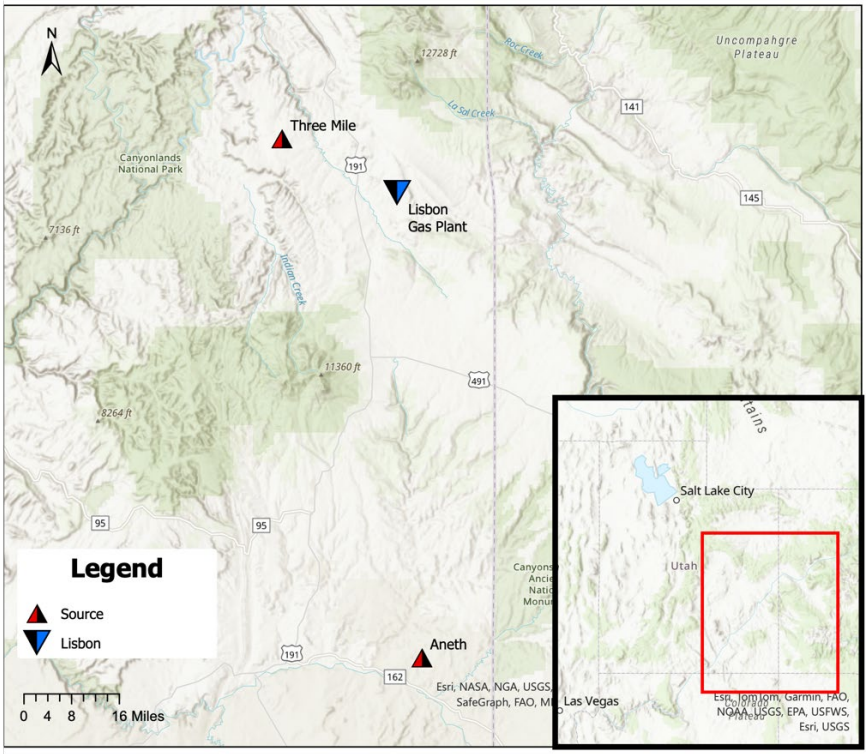

Figure 1: The regional map of the Lisbon Valley, including the locations of sources of fluids piped to the plant.

The Southwest Partnership

The Southwest Regional Partnership on Carbon Sequestration (SWP) is one of seven regional partnerships established in 2003 by the U.S. Department of Energy (DOE) to study carbon management strategies. Since the creation of the partnership, the CSI team has contributed to SWP through a number of studies including the *Geologic Model Development and Numerical Simulation of the Aneth Site, Utah* (DE-FC26-05NT4259) located in the southwestern part of the Paradox Basin in the Aneth oil and gas field operated by Resolute Natural Resources and Navajo Nation Oil & Gas Co., Inc. The objective of this project is to demonstrate combined CO_2 storage and enhanced oil recovery (EOR) potential. The CSI team at EGI was extensively involved in developing a geological model of the field and conducting numerical simulations to demonstrate efficacy of CO_2 sequestration technologies within producing oil reservoirs. In this project, EGI focused on developing a site-specific geologic model to better understand and design CO_2 storage specifically tailored to oil reservoirs. The research was primarily focused on gathering and using data specific to the Aneth site, but it is anticipated that the results of the Aneth research will be useful in a variety of CO_2 EOR projects and oil fields elsewhere. Geologic sequestration of CO_2 in the Aneth field includes injection of up to 0.15 MMt/yr CO_2 with a minimum injection duration of one year.

Well logs were acquired, digitized, and integrated into the model to review petrophysical data for estimating essential properties such as porosity and permeability. Numerical simulations were conducted on a conceptual model built on geological data from Section 13 and 14 of the Aneth field in southeastern Utah, as well as studies on the sensitivity of injectivity, maximal pressure, and the effect of hysteresis and water-alternating-gas (WAG). According to our estimation of the permeability and resulting numerical simulations, the maximum injection rate should not exceed 0.25 million metric tons per year (MMt/yr). To achieve a 1 MMt/yr injection rate, the permeability should be at least 5 times higher than our estimation, although 10 times higher permeability may be more reasonable. The highest pressure induced by injection was investigated according to the number of wells. The effects of WAG schemes and hysteresis are weak on dissolution trapping mechanisms. This conclusion is site and model specific and should be investigated using alternative models.

Paradox Emerging Oil Play

In the northern region of the Paradox Basin, the *Improving Production in the Emerging Paradox Oil Play* (DE-FE0031775) project aims to assess and evaluate optimum strategies to drill economic wells in the structurally complex, but highly prospective, emerging unconventional Paradox Basin oil play, in particular the Pennsylvanian Paradox Formation's Cane Creek shale and adjacent clastic zones. This objective was accomplished through geologic characterization, coupled model development, determination of optimum well locations and trajectories, and development of a tactical stimulation strategy.

Geologic characterization involved understanding and studying the geologic properties and characteristics of the Paradox Play region. This included assessing the geological features, rock formations and properties, petrophysical and seismic data collection and analysis, and simulation development. The results of the geologic characterization included fracture toughness values across scales and demonstrates that nanoindentation tests provide a rapid and reliable method for predicting macro-scale fracture toughness.

Coupled model development involved creating and refining simulation models for specific areas of interest. Incorporation of historical data, permeability modifications, and the development of a capillary pressure to relative permeability function were significant additions to the modeling process followed by iterations of the discrete fracture network (DFN) to better align simulation outcomes with historical production data. Significant finding included the insensitivity to changes in the DFN and fault transmissibility but high sensitivity to matrix permeability and porosity. Changing the hydraulic fracture stages and density had the biggest effect on both production and bottom hole pressure and allowed the model to match historical data. To determine optimum well locations and trajectories, the team calculated the Coulomb failure function for a matrix of strikes and dips which shows there are several quite attractive candidates for which fault orientation may satisfy the fault hypothesis. Additionally, the team explored the deployment of downhole seismometers with a focus on enhancing Paradox well data.

Direct Air Capture

EGI, University of Utah, partnered with InnoSense LLC on the *High-Performance, Hybrid Polymer Membrane for Carbon Dioxide* (DE-FE0031968) project in response to the DOE's call for the development of novel DAC materials that demonstrate high capacities for CO_2 in the air. InnoSense LLC led this project to develop high-performance, hybrid polymer membranes (HypoMemTM) for CO_2 separation from ambient air. The CSI/EGI team contributed through computer simulation modeling based on project test data/results to optimize separation process systems for CO_2 capture from ambient air, and basic level techno-economic analysis (TEA) and life cycle analysis. The results determined parameters which strongly influence factors such as purity, recovery and energy requirements, membrane area required, and the total annualized cost. Overall, this study suggests that utilizing a high-selective, non-porous, low surface area, membrane-based CO_2 capture from the air could be a potential new technology for DAC in addition to sorbent-based systems.

Capture at the Hunter Power Plant

Techno-Economic Analysis of Amine-based CO_2 Capture Technology: Hunter Plant Case Study (CarbonSAFE Project, DE-FE0029280), a Carbon Capture and Storage (CCS) feasibility study, was conducted by members of the CSI team in 2022. This project evaluated the potential for CCS in a geologic formation adjacent to PacificCorp's Hunter Plant. The evaluation included the creation of projected performance as well as the startup and ongoing expenses related to installing CCS in the Hunter Plant, which burns subbituminous, low-sulfur coal. Using a commercially available amine-based system as the foundation for the capture technology, this study effort also involved the evaluation of multiple capture levels. The KM-CR Process® with KS-1TM solvent from Mitsubishi Heavy Industries (MHI) served as the foundation for the system design and cost estimates. At higher capture rates, the total cost of capture ($/metric ton of CO_2 removed) is lower due to economies of scale. The price of capturing CO_2 from Hunter 3 with a purity of more than 95% ranges from $50, $61, and $74 per metric ton of CO_2 removed.

Regional Direct Air Capture

The upcoming *ASU Regional Direct Air Capture (DAC) Hubs* (DE-FOA0002735) project will be led by ASU to pursue a front-end engineering design (FEED) for a multi-site regional DAC Hub located in the four corners of the southwest of the United States. The University of Utah, EGI, will partner as the lead on the Utah site, contributing to both technical tasks and community benefits plan (CBP) implementation.

Prefeasibility study of Carbon Capture and Storage from Hunter and Huntington Power Plants
CarbonSAFE Rocky Mountain Phase I: Ensuring Safe Subsurface Storage of Carbon Dioxide in the Intermountain West (DE-FE0029280) was conducted as part of the DOE's Carbon Storage Assurance and Facility Enterprise (CarbonSAFE) program. The goal was to develop a template protocol for existing and future coal-fired as well as natural-gas-fired plants in the Rocky Mountain states. Hunter Power Plant in central Utah was identified as the primary source of CO_2 for this study and the nearby Huntington Power Plant, also operated by Rocky Mountain Power, was evaluated as a secondary source of CO_2. Hunter Plant was chosen because of an interest in CO_2 capture technology by the plant operator, Rocky Mountain Power, and because it is a representative example of a typical coal-fired generating station in the Rocky Mountain west. Amine-based and cryogenic-based capture assessments were performed for approximately 3 MMt/yr for one of the boiler units at the Hunter Plant, yielding cost of capture estimates of $56/metric ton and $41.50/metric ton.

A high-level technical sub-basinal evaluation was performed on the area surrounding the Hunter and Huntington Power Plants to verify CO_2 storage capacity and integrity. Initial geologic characterization efforts focused on sites immediately adjacent to the Hunter Plant, including the deep eolian Navajo Sandstone, which in outcrop and core from other locations indicates high permeability and high porosity. A comprehensive analysis of the reservoir and seals was conducted, providing data to the model simulation and risk assessment groups on the project. CO_2 capacity estimates for the Navajo Sandstone approximately 18 kilometers from the Hunter Plant are well in excess of the 50 million metric tons goal of the project. Area of Review Delineation and Risk Assessment on the Navajo, associated seals and shallow groundwater aquifers identified the most significant risks and mitigation options.

2.2 - Site History

The Lisbon area in San Juan County, Utah, has a rich history of natural resource production, particularly in oil, gas, and copper mining, although all of the wells in the maximum monitoring area for this MRV Plan are plugged and abandoned or shut-in. This region is part of the Paradox Basin, known for its complex geological structures and significant hydrocarbon resources. Over the decades, extensive exploration and production activities have shaped the economic and environmental landscape of the Lisbon Valley (Seneshen et al., 2010).

Early Oil and Gas Exploration

The discovery of oil in the Lisbon area dates back to January 4, 1960, when The Pure Oil Company completed the No. 1 N.W. Lisbon 'A' well in Section 10. This well flowed 587 barrels of oil per day from the upper Devonian McCracken Sandstone, marking the beginning of significant hydrocarbon exploration and production in the region. The success of this well was quickly followed by another significant discovery, the Mississippian oil well Pure No. 1 N.W. Lisbon 'B', which produced 406 barrels of oil and 6,382 MCFG per day from the Mississippian formation and 287 barrels of oil per day from the McCracken Sandstone (Matheny, 1978; Bradley, 1975).

The Lisbon Field's geological complexity required extensive subsurface and seismic exploration to fully understand and exploit its hydrocarbon potential. These efforts were successful as subsequent discoveries in the Mississippian formations led to substantial production. Since its discovery, the Lisbon Field has produced over 51.5 million barrels of oil and 811.5 billion cubic feet of gas as of January 2024 (Department

of Natural Resources, 2024). The produced gas is processed on-site to extract valuable components like propane, butane, and natural gasoline, while the remaining dry gas is reinjected into the reservoir to maintain pressure and enhance oil recovery.

The geological setting of the Lisbon Field, within the Paradox Fold and Fault Belt, significantly influenced the hydrocarbon trapping mechanisms. The primary hydrocarbon-producing formations include the Mississippian Redwall Limestone and the Devonian McCracken Sandstone. The Redwall Limestone is particularly noteworthy for its karsted upper zone, porous middle dolomite zone, and tight lower dolomite zone, which collectively contribute to its reservoir quality and production potential.

The strategic use of modern exploration techniques, such as high-quality two-dimensional and three-dimensional seismic data, has been instrumental in identifying new drilling targets and optimizing hydrocarbon recovery in the Lisbon area. These advancements, combined with a thorough understanding of the area's complex structural geology, have solidified the Lisbon Field as a significant contributor to Utah's oil and gas production (Bradley, 1975; Chidsey, 2005).

Geological and Structural Features

The Lisbon Field is situated within the structurally complex Paradox Fold and Fault Belt. The local structure consists of a faulted, asymmetrical northwest-southeast trending anticline, with steeper dips on the northeast flank paralleling a major normal longitudinal fault. This structural complexity is due to the region's salt tectonics, which has played a crucial role in hydrocarbon trapping. The primary reservoir formations include the Mississippian Redwall Limestone and the Devonian McCracken Sandstone (Bradley, 1975; Chidsey, 2005).

Stratigraphy and Production

The stratigraphy of the Lisbon Field is varied, encompassing formations from the Cambrian to the Triassic periods. The Mississippian Redwall Limestone is the primary hydrocarbon-producing formation, characterized by an upper karsted limestone zone, a middle porous dolomite zone, and a lower tight dolomite zone. The middle dolomite zone is the main reservoir due to its higher porosity and permeability. Production from the Redwall at Lisbon has been substantial since the field was discovered in 1960 (Bradley, 1975; Chidsey, 2005). However, the field has been in production decline for decades.

Advancements in Exploration Techniques

Extensive 2D and 3D seismic exploration measurements have been crucial in understanding the complex geology of the Lisbon Field. Modern exploration techniques, including surface geochemical surveys, have been employed to identify new drilling targets and optimize hydrocarbon recovery. These advancements have allowed for more efficient exploitation of the region's resources, contributing to the success of new wells drilled in the area.

Copper Mining in Lisbon Valley

In addition to hydrocarbon production, the Lisbon Valley is also known for its copper mining activities. The Lisbon Valley Copper Mine has been operational under various ownerships since 1998. The mine plan covers 4,480 acres, with additional exploration activities authorized over 5,430 acres. The mining operations involve conventional open-pit methods, with copper ore being processed through heap leaching and solvent extraction-electrowinning techniques to produce high-purity copper cathodes. The Bureau of

Land Management (BLM) oversees environmental impact assessments and regulatory compliance for these operations (Sheehan, 2024).

Environmental and Regulatory Aspects

The development of natural resources in the Lisbon area is subject to stringent environmental and regulatory oversight. The BLM and other regulatory bodies ensure that exploration and production activities comply with environmental standards and minimize impacts on the surrounding ecosystem. This includes monitoring air and water quality, managing waste materials, and conducting reclamation activities to restore disturbed lands (Sheehan, 2024).

Summary

The Lisbon area in Utah has a long and productive history of natural resource extraction, primarily focused on oil, gas, and copper. The region's complex geology and rich resource base have attracted significant exploration and production activities, contributing to its economic development. Despite the relative success of extracting natural resources from the Lisbon area, however, all of the wells within the maximum monitoring area have been shut-in or plugged and abandoned. This leaves no fluids being currently produced near the injection location.

2.3 - Geology

The Lisbon area in Utah, situated within the Paradox Basin, presents a remarkable geological and stratigraphic record that spans from the Paleozoic to the Mesozoic eras. This region contains a diverse array of sedimentary formations summarized in the chronostratigraphic chart in Figure 2, and geologic outcrops in the area displayed in the map in Figure 3.

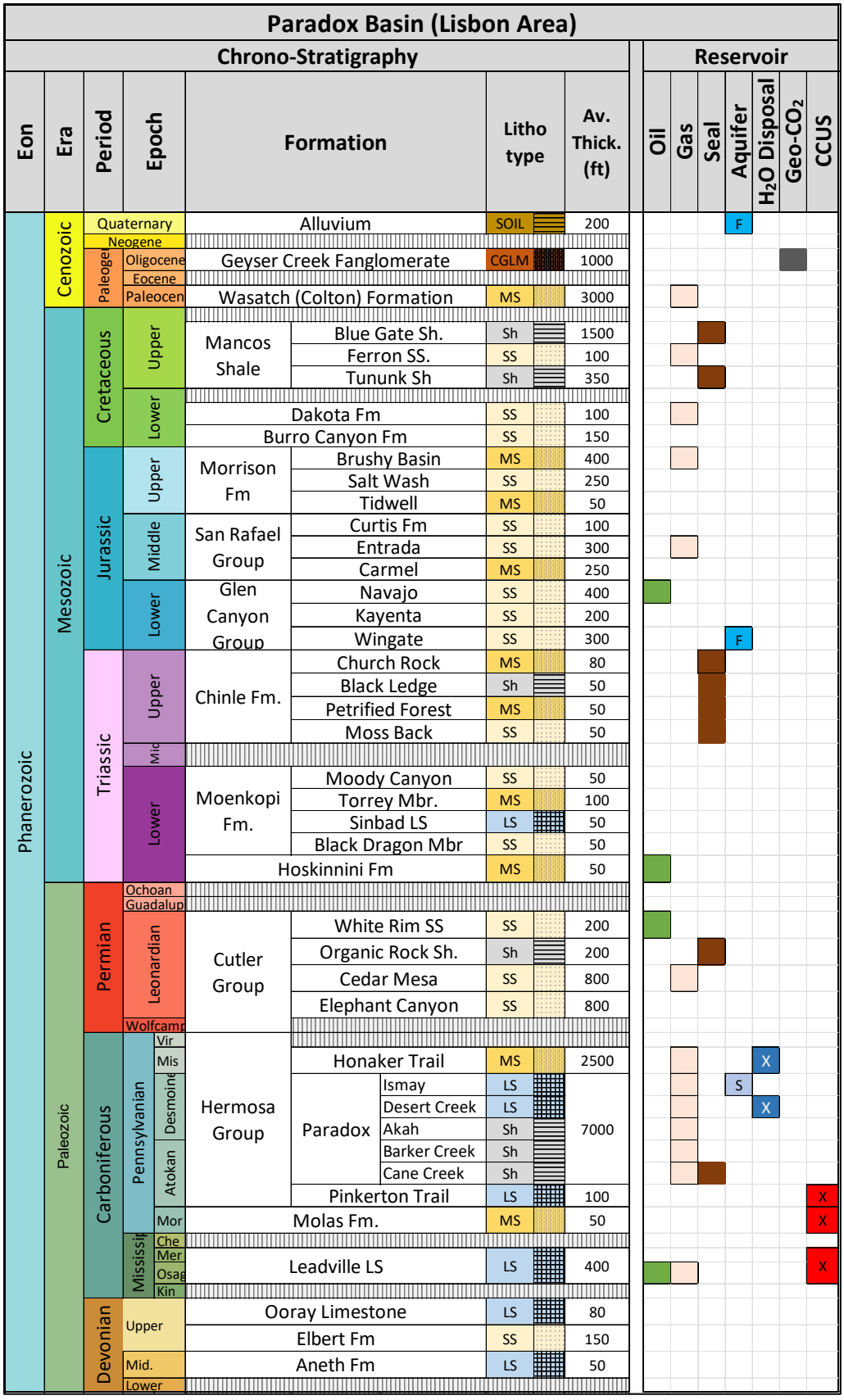
Paradox Basin (Lisbon Area)
Chrono-Stratigraphy
Reservoir
Eon
Era
Period
Epoch
Formation
Litho type
Av. Thick. (ft)
Oil
Gas
Seal
Aquifer
H2O Disposal
Geo-CO2
CCUS
Phanerozoic
Cenozoic
Mesozoic
Paleozoic
Quaternary
Alluvium
SOIL
200
Neogene
Paleogene
Oligocene
Geyser Creek Fanglomerate
CGLM
1000
Eocene
Paleocen
Wasatch (Colton) Formation
MS
3000
Cretaceous
Upper
Mancos Shale
Blue Gate Sh.
Sh
1500
Ferron SS.
SS
100
Tununk Sh
Sh
350
Lower
Dakota Fm
SS
100
Burro Canyon Fm
SS
150
Jurassic
Upper
Morrison Fm
Brushy Basin
MS
400
Salt Wash
SS
250
Tidwell
MS
50
Middle
San Rafael Group
Curtis Fm
SS
100
Entrada
SS
300
Carmel
MS
250
Lower
Glen Canyon Group
Navajo
SS
400
Kayenta
SS
200
Wingate
SS
300
Triassic
Upper
Chinle Fm.
Church Rock
MS
80
Black Ledge
Sh
50
Petrified Forest
MS
50
Moss Back
SS
50
Mid
Lower
Moenkopi Fm.
Moody Canyon
SS
50
Torrey Mbr.
MS
100
Sinbad LS
LS
50
Black Dragon Mbr
SS
50
Hoskinnini Fm
MS
50
Ochoan
Guadalup
Permian
Leonardian
Cutler Group
White Rim SS
SS
200
Organic Rock Sh.
Sh
200
Cedar Mesa
SS
800
Elephant Canyon
SS
800
Wolfcamp
Carboniferous
Pennsylvanian
Vir
Mis
Honaker Trail
MS
2500
Desmoine
Hermosa Group
Paradox
Ismay
LS
7000
Desert Creek
LS
Akah
Sh
Barker Creek
Sh
Cane Creek
Sh
Atokan
Pinkerton Trail
LS
100
Mor
Molas Fm.
MS
50
Mississip
Che
Mer
Osag
Leadville LS
LS
400
Kin
Devonian
Upper
Ooray Limestone
LS
80
Elbert Fm
SS
150
Mid.
Aneth Fm
LS
50
Lower
F
X
S

Figure 2: Chronostratigraphic chart of the Paradox Basin, describing the lithology and potential applications for production and storage.

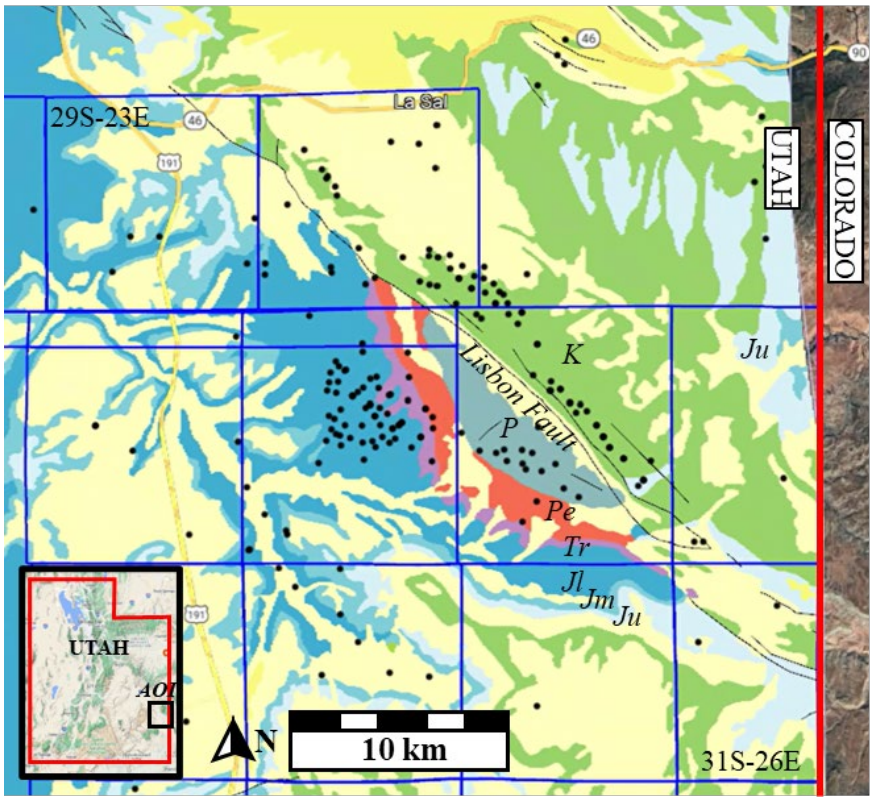

Figure 3: Geologic Map in the Lisbon area indicating the location of the oil and gas wells, the dominant Lisbon Fault, and the formation outcrops Ju: Upper Jurassic, Jm: Mid-Jurassic, Jl: Lower Jurassic, Tr: Triassic, Pe: Permian, P: Pennsylvanian.

Cretaceous

In the Paradox Basin near Monticello, Utah, the Dakota Formation and the Burro Canyon Formation are significant geological units from the Cretaceous period (Repenning and Page 1956; Mcpherson et al. 2006; Kirkland et al. 2016). The Dakota Formation is characterized by its sandstones, shales, and occasional coal beds, indicating deposition in fluvial and coastal environments with river channels, floodplains, and swamps. This formation marks the initial transgression of the Cretaceous Western Interior Seaway. Underlying the Dakota Formation, the Burro Canyon Formation consists of conglomerates, sandstones, and mudstones, representing fluvial and deltaic environments with evidence of ancient river systems and floodplain deposits. Together, these formations provide a record of the transition from terrestrial to marine conditions in the early Cretaceous period in the Paradox Basin. The Cretaceous outcrops are observed in the southern sector of the Lisbon area and as the hanging wall, in the northern rim of the Lisbon Fault.

Upper Jurassic

The Morrison Formation is a Late Jurassic sedimentary sequence (Kirkland et al. 2016), divided into three primary submembers: Brushy Basin, Salt Wash, and Tidwell. The Brushy Basin Member is characterized by its variegated mudstones and abundant dinosaur fossils, indicative of deposition in floodplain and

lacustrine environments. The Salt Wash Member consists of interbedded sandstones and mudstones, representing braided river systems and associated floodplains, known for its well-preserved fluvial channels. The Tidwell Member, at the base, comprises siltstones and sandstones with calcareous and gypsiferous beds, reflecting a mix of fluvial, deltaic, and shallow marine environments. Together, these submembers document a diverse range of depositional settings from terrestrial to marginal marine, making the Morrison Formation a key unit for understanding the Late Jurassic paleoenvironment and paleobiology in the Paradox Basin. The outcrops of the Morrison Formation follow conformably the northern contour of the Cretaceous unit outcrops.

Middle Jurassic

The San Rafael Group is a Middle Jurassic geological unit comprising the Curtis Formation, Entrada Sandstone, and Carmel Formation (Rasmussen and Rasmussen 2009), each with distinct depositional environments and reservoir properties. The Curtis Formation consists of marine sandstones and siltstones, exhibiting moderate porosity and permeability suitable for hydrocarbon reservoirs. The Entrada Sandstone, characterized by large-scale cross-bedded aeolian sandstones, features high porosity and permeability due to its well-sorted and loosely cemented grains, making it an excellent reservoir rock. The Carmel Formation, with its interbedded mudstones, siltstones, limestones, and gypsum, generally has lower porosity and permeability, potentially acting as a cap rock or barrier in subsurface fluid flow. Collectively, these formations provide a comprehensive record of marine, desert, and coastal environments during the Middle Jurassic and hold significant potential for resource exploration due to their varied reservoir characteristics.

Lower Jurassic

The Glen Canyon Group (Lessentine 1965; Rice 2003; Trudgill 2011) comprises three prominent Triassic to Jurassic formations: the Navajo Sandstone, Kayenta Formation, and Wingate Sandstone. The Navajo Sandstone is renowned for its massive, cross-bedded aeolian (wind-blown) sandstones, which exhibit high porosity and permeability due to their well-sorted, rounded grains, making it an excellent reservoir rock for groundwater and hydrocarbons. The Kayenta Formation consists of interbedded sandstones, siltstones, and mudstones, representing fluvial environments with moderate porosity and permeability, suitable for secondary reservoirs or aquifers. The Wingate Sandstone, characterized by its tall, cross-bedded sandstone cliffs formed in an ancient desert environment, also has high porosity and permeability, comparable to the Navajo Sandstone. Together, these formations record a transition from arid desert to fluvial environments and are significant for their excellent reservoir properties, offering substantial potential for resource exploration and groundwater storage.

Triassic

The Chinle Formation, (Lessentine 1965; Leake et al. 2005; Trudgill 2011) a Late Triassic unit, is notable for its colorful sedimentary layers and rich fossil content, divided into the Church Rock, Black Ledge, Petrified Forest, and Moss Back members. The Church Rock Member is characterized by its reddish sandstones and mudstones, indicating fluvial and floodplain environments with moderate porosity and permeability. The Black Ledge Member, composed of interbedded sandstones and shales, has variable porosity and permeability, reflecting deposition in both fluvial and lacustrine settings. The Petrified Forest Member, known for its multicolored mudstones and significant petrified wood, generally has low permeability and porosity due to its fine-grained nature, acting more as a confining layer. The Moss Back Member, with its coarse sandstones and conglomerates, indicates high-energy river environments and

exhibits high porosity and permeability, making it a potential reservoir rock. Together, these submembers provide insights into diverse depositional environments from river systems to floodplains and lakes, with varied reservoir properties significant for groundwater and hydrocarbon exploration.

The Moenkopi Formation is an Early to Middle Triassic sedimentary sequence with notable submembers including the Moody Canyon, Torrey, Sinbad Limestone, and Black Dragon members. The Moody Canyon Member is characterized by fine-grained sandstones, siltstones, and mudstones deposited in fluvial and deltaic environments, exhibiting moderate porosity and permeability. The Torrey Member consists of siltstones and mudstones with occasional sandstones, reflecting low-energy environments like floodplains and shallow marine settings, generally having lower porosity and permeability. The Sinbad Limestone Member, composed of thin-bedded limestones and dolomites, indicates a shallow marine environment and features variable porosity and permeability depending on the degree of fracturing and dolomitization. The Black Dragon Member, marked by its red beds of sandstones and siltstones, represents fluvial and tidal flat deposits with moderate to good porosity and permeability. Together, these submembers reflect a range of depositional environments from fluvial to shallow marine, with varying reservoir quality.

The Hoskinnini Formation is a Triassic-aged unit composed primarily of red and orange sandstones, siltstones, and shales, indicative of deposition in fluvial and deltaic environments. The formation is characterized by its fine to medium-grained sandstones, which generally exhibit low to moderate porosity and permeability due to the presence of clay and silt that fill pore spaces and reduce fluid flow.

Permian

The Cutler Group (Blakey 1990) is a Permian geological unit comprising the White Rim Sandstone, Organ Rock Shale, Cedar Mesa Sandstone, and Elephant Canyon Formation. The White Rim Sandstone, known for its well-sorted, fine-grained sandstones, exhibits high porosity and permeability, making it an excellent reservoir rock for hydrocarbons and groundwater. The Organ Rock Shale, characterized by its red, fine-grained shales and siltstones, has low permeability and porosity, serving more as a confining layer than a reservoir. The Cedar Mesa Sandstone, consisting of massive, cross-bedded sandstones, also features high porosity and permeability due to its coarse grain size and well-sorted nature, making it a prime target for hydrocarbon exploration. The Elephant Canyon Formation, with its interbedded sandstones, shales, and limestones, shows variable porosity and permeability, dependent on the specific lithology and degree of fracturing.

Pennsylvanian

The Hermosa Group (Hite and Buckner 1981; Blakey 1990; Trudgill 2011; Morgan 2015) is a prominent Pennsylvanian to Permian sedimentary sequence, consisting of the Honaker Trail Formation, Paradox Formation (including its submembers Desert Creek, Akah Shale, Barker Creek Shale, and Cane Creek Shale), and Pinkerton Trail Formation. The Honaker Trail Formation is characterized by interbedded limestones, sandstones, and shales, displaying moderate porosity and permeability, suitable for hydrocarbon reservoirs. The Paradox Formation, known for its cyclic deposits of anhydrite, halite, and shales, features variable reservoir qualities; the Desert Creek exhibits high porosity and permeability due to its carbonate build-ups, making it a prime hydrocarbon target, while the Akah, Barker Creek, and Cane Creek Shales generally have lower permeability, acting as seals or secondary reservoirs, although the Cane Creek Shale is an organic-rich formation that has been commercially developed for condensate and gas

production in the central region of the Paradox Basin. In the geological model for the Lisbon area, the base of the Cane Creek is considered the top of the seal rock. The Pinkerton Trail Formation consists of interbedded limestones and shales, typically showing moderate porosity and permeability, as observed from petrophysical logs and is included as part of the potential CO_2 reservoir.

The Molas Formation is a Mississippian to Pennsylvanian unit that typically serves as a transitional layer between older carbonate rocks and overlying siliciclastic sequences. This formation is characterized by its red and green shales, siltstones, and occasional sandstone beds, indicating deposition in fluvial to shallow marine environments. The Molas Formation generally exhibits low to moderate porosity and permeability due to its fine-grained, shaly nature, which limits its potential as a primary reservoir rock. However, the occasional sandstone beds within the formation can have better reservoir qualities, albeit often discontinuous and variable. Commercial interest in the Molas Formation is typically lower compared to adjacent formations with better reservoir properties, but it can still play a role in the regional stratigraphy and hydrocarbon system as a secondary target or seal.

Mississippian

The Leadville Limestone (Blakey 1990; Blakey et al. 1996; Whidden et al. 2014) is a Mississippian-aged carbonate formation characterized by thick, massive limestone and dolomite beds, often interbedded with chert. This formation was deposited in a shallow marine environment and is known for its excellent reservoir qualities due to its high porosity and permeability, especially where secondary porosity has developed through processes like dolomitization and fracturing. In the case of the Lisbon area, these features lead to high potential for CCS. The combination of primary porosity from the original deposition and secondary porosity from diagenetic alterations enhances its capacity to store and transmit fluids.

Devonian

The Ouray Limestone is a Devonian-aged carbonate formation characterized by its thick, fossiliferous limestone beds, often interspersed with dolomite. Deposited in a shallow marine setting, the Ouray Limestone exhibits variable porosity and permeability. Primary porosity is typically low due to the compact nature of the limestone. The Elbert and Aneth Formations underly Ouray limestone.

2.4 - Facility Information and CCS System

Reporter Number

The greenhouse gas reporting program (GHGRP) ID number is 523298.

UIC Injection Well Identification Numbers

This plan pertains to the acid gas injection (AGI) well Lisbon Unit D-716, API (4303731034), underground injection control (UIC) permit 429.1.

UIC Permit Class

The AGI well is permitted by the Utah Division of Oil, Gas, and Mining (DOGM) as UIC Class II AGI well. All oil- and gas-related wells within the Lisbon Field, including both injection and (shut in) production wells, are regulated by DOGM, which has primacy of UIC Class II wells.

Plant Operations

The process at the GNG Lisbon Gas Processing Plant involves an integrated system of cooling, separation, and solvent scrubbing to efficiently capture and prepare CO_2 for sequestration. The detailed process involving absorbers, regenerators, and supporting equipment ensures that CO_2 is effectively separated from natural gas and readied for geological storage. A typical process diagram for natural gas production and CO_2 capture facility is shown in Figure 4. Note that in the case of the Lisbon Gas Processing Plant, the production is taking place at other fields and the fluids are piped to the plant.

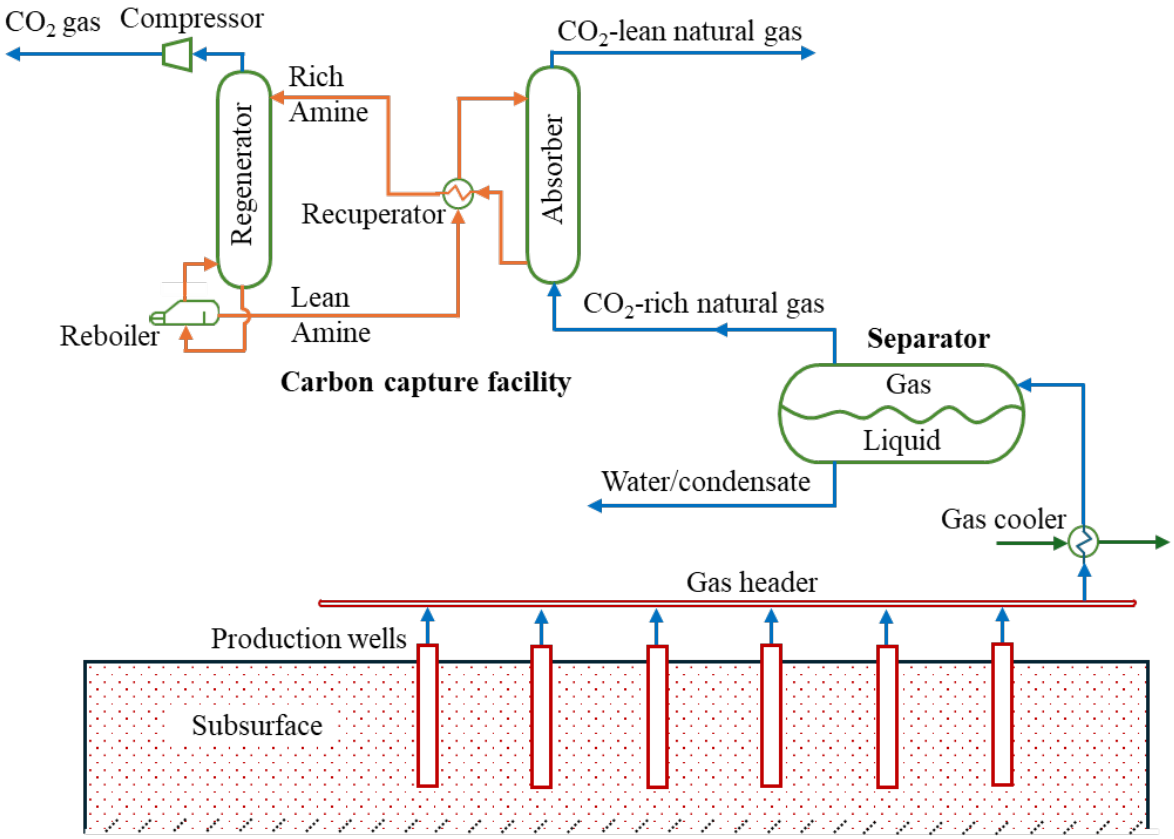

Figure 4: A Simplified Schematic of Natural Gas Production and Carbon Capture Facility.

Natural gas is collected in a header from various production wells within the gas field. Before the CO_2-rich natural gas is sent to the carbon capture facility, it undergoes several preprocessing steps. These include cooling the gas and separating the gas and liquid components (hydrocarbon condensate and water) using separators.

Sources of H_2S and CO_2

The Lisbon Gas Processing Plant processes natural gas, sourced from other fields, which serves as the source of both H_2S and CO_2. The natural gas production process involves the extraction and refinement of raw natural gas, during which H_2S and CO_2 are separated from the hydrocarbon stream. These acid gases

are by-products of the gas sweetening process, which is necessary to meet pipeline quality specifications and environmental regulations.

Capture Technologies

At the Lisbon Gas Processing Plant, advanced capture technologies are implemented to isolate CO_2 from the processed natural gas. The primary technology used is amine gas treating, also known as amine scrubbing. This process involves the use of an aqueous amine solution to absorb CO_2 from the gas stream. The rich amine solution, now containing the absorbed acid gases, is then regenerated in a stripping column, releasing purified CO_2 for sequestration. This process involves two main processing units: the absorber and the regenerator (or stripper).

Absorber:

- The absorber captures CO_2 from the CO_2-rich natural gas using a lean aqueous amine solvent.
- CO_2-rich natural gas enters the bottom of the absorber, while the lean amine stream enters from the top.
- As the gas ascends, CO_2 is absorbed by the amine solvent, resulting in CO_2-lean natural gas exiting from the top of the absorber.
- The rich amine stream, now containing absorbed CO_2, exits from the bottom of the absorber.

Regenerator (Stripper):

- The regenerator separates the absorbed CO_2 from the rich amine solvent.
- The regenerated amine solvent is recycled back to the absorber, supplemented by fresh makeup amine.
- The separated CO_2, collected from the top of the regenerator, is then prepared for geological sequestration.

Supporting Equipment

- **Pumps and Compressor**s: These are essential for circulating the amine solvent and compressing the captured CO_2 for transportation.
- **Heat Exchangers:** These are used to optimize the thermal efficiency of the process. A recuperator exchanges heat between the cold rich amine stream and the hot lean amine stream.
- **Reboiler:** Located at the bottom of the regenerator, the reboiler heats the liquid to create vapor, aiding in the CO_2 separation process.
- **Cooling Systems:** Additional cooling is often required at the top of the absorber to maintain a lower temperature, enhancing the absorption efficiency.

Operating Conditions

- The absorber operates at lower temperatures to improve the absorption efficiency of CO_2 into the lean amine solvent.
- The regenerator operates at higher temperatures to release CO_2 from the rich amine solvent.

Design Considerations

The design of the absorber and regenerator, including their heights, diameters, and packing materials, depends on the gas flow rates, CO_2 concentration in the gas, and the concentration of amine in the aqueous solution. This ensures the optimal performance of the CO_2 capture process.

Proposed Injection Parameters

The captured CO_2 will be transported to a primary AGI well for geological sequestration. The injection parameters are designed to ensure safe and efficient storage of the gases in the subsurface. These parameters include:

- **Injection Rate:** The rate at which treated acid gas will be injected into the well, carefully calibrated to match the capacity of the geological formation and avoid over-pressurization. This rate is anticipated to be 4-12 million standard cubic feet per day (MMSCFD).
- **Injection Pressure:** The pressure at which the gases will be injected, optimized to ensure maximum sequestration efficiency while maintaining the integrity of the reservoir.
- **Injection Depth:** The depth of the injection well, targeting a suitable geological formation known for its capacity to securely store acid gases. The injection will be into the Leadville Formation with an approximate depth of 8200 ft.
- **Monitoring Protocols:** Continuous monitoring of injection parameters to ensure compliance with safety standards and to detect any anomalies promptly.

Pipeline Analysis

The pipeline infrastructure from the Lisbon Gas Processing Plant to the primary AGI well is a critical component of the CCS system. This pipeline is designed to safely transport the compressed CO_2 over the required distance. Key considerations in the pipeline design and analysis include:

- **Pipeline Route:** The selected route minimizes environmental impact and avoids densely populated areas to enhance safety and regulatory compliance.
- **Material Selection:** The pipeline is constructed using materials resistant to the corrosive nature of CO_2, ensuring long-term durability and safety.
- **Pressure Management:** The pipeline system includes pressure management controls to maintain optimal pressure levels during transportation.
- **Leak Detection Systems:** Advanced leak detection technologies are employed to promptly identify and address any leaks, ensuring environmental protection and operational safety.

3.0 - Delineation of the Maximum Monitoring Area

3.1 - Petrophysical Description

The petrophysical analysis consisted of verifying the data availability. Based on the petrophysical data available, summarized in Table 1 (0 = data not available 1 = digital log data (LAS) available in the Leadville), it was determined that the primary reference for porosity was the acoustic log (DT), which most of the wells have (Table 1).

Table 1: Wells containing quantitative wireline logs in the region.

GR	RHOB	NPHI	DT	API Well Number	Well Name
1	0	0	1	4303716219	Big Indian Unit 1
1	0	0	1	4303711345	Big Indian Unit 2
1	0	0	1	4303711346	Big Indian Unit 5
1	0	0	1	4303730005	Chevron Fed 1

1	0	1	1	4303711356	Cordillera St 1
1	0	0	1	4303730382	Federal 13-30
1	0	0	1	4303730999	Federal 21-4
1	1	1	1	4303730572	Govt Evelyn Chambers 1
1	1	1	1	4303730612	Govt Evelyn Chambers 2
1	0	1	1	4303730206	La Sal Federal 1
1	1	1	1	4303731351	Lisbon B-614A
1	0	0	1	4303716242	Lisbon B-616
0.5	0	0	1	4303716241	Lisbon B-69
1	0	1	1	4303730082	Lisbon B-814
1	0	0	1	4303716243	Lisbon B-815
1	0	0	1	4303730054	Lisbon B-84
0.5	0	0	1	4303715769	Lisbon B912
1	0	0	1	4303716248	Lisbon C-814
1	0	0	1	4303716246	Lisbon C-84
1	0	0	1	4303716251	Lisbon D-89
1	0	0	1	4303715768	Lisbon Fed 2-21F
1	1	1	1	4303730436	Lisbon Federal 21-3
0.5	0	0	1	4303716469	Lisbon U B-610
1	0	0	1	4303710340	Lisbon Valley 1-22C (B622)
1	0	0	1	4303710807	Little Valley 1
1	0	0	1	4303730029	Little Valley Fed 1
0.5	0	0	1	4303716471	NW Lisbon USA A-2 (D-810)
0.5	0	0	1	4303716468	NW Lisbon USA B-1 (B-614)
0.5	0	0	1	4303711339	NW Lisbon USA C-2 (B63)
0.5	0	0	1	4303716470	NW Lisbon USA-C3 (C93)
1	0	0	1	4303730044	State Gulf 1

Data preprocessing consisted in rescaling the gamma ray (GR) logs by using the equation for featured rescaling. This processing allowed the homogenization process of having the GR under the same range, being comparable between wells. For instance, the histograms in Figure 5 correspond to GR reading in the well Lisbon B-69. The raw GR data is acquired within a range of 0 to 12 gAPI (the units for the gamma ray log, whereas the rescaled values are from 0 to 120 gAPI, which are within the expected values in the industry.

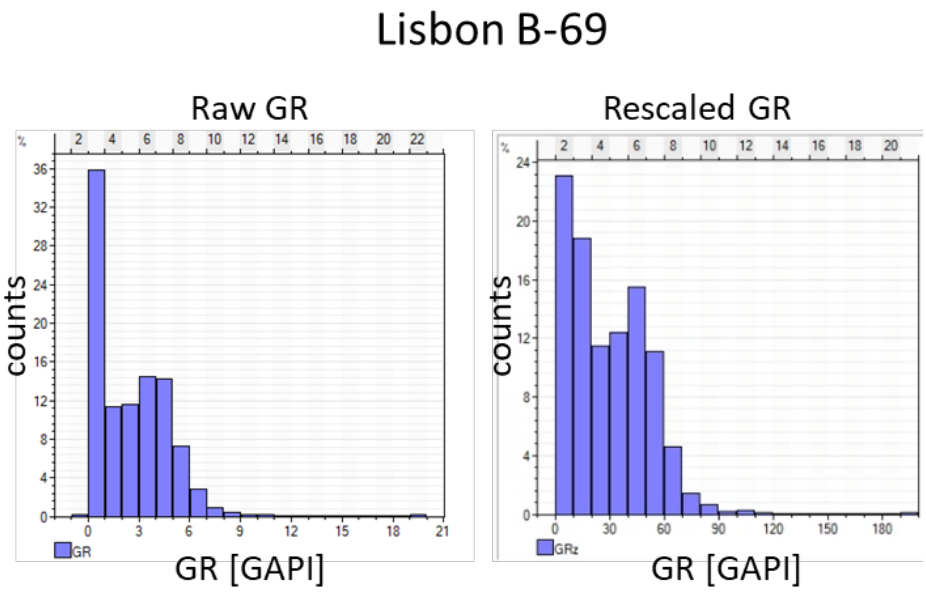

Figure 5: Histograms of GR logs for raw and rescaled data.

The Sonic porosity was calculated using the conventional equation, calibrating the matrix transit time DT_{ma} to match the porosity curve from neutron porosity. $SPHI = (DT_c - DT_{ma}) / (DT_f - DT_{ma})$, where DT_c is the log reading for compressional Delta T, DT_{ma} is the matrix slowness, and DT_f is the fluid slowness, assumed 189 us/ft. The matrix transit time was defined as 44 us/ft from the correlation to neutron porosity, in Figure 6a and the depth log in Figure 6b.

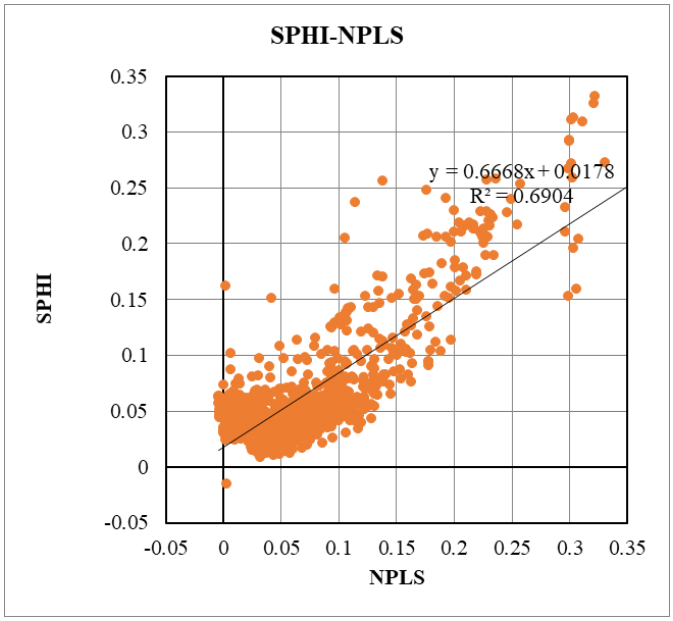

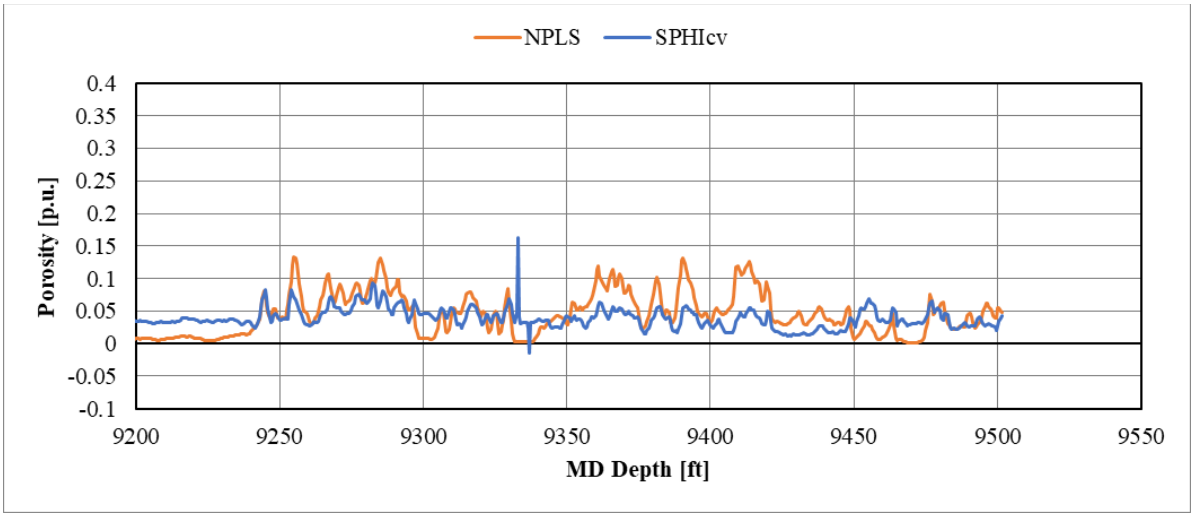

Figure 6: a) SPHI Correlation vs NPHI b) log difference between SPHI and NPHI

Once the GR and Sonic porosity curves have been calibrated, the model is extrapolated to the other wells in the area, and the static geo-model is built, identifying the reservoir rock including the Pinkerton, Molas, and Leadville Formations, and the lower section of the Paradox Formation (base of Cane Creek Formation) as the seal rock. Figure 7 shows the type well (Lisbon B-69) in the seal and reservoir sections. The calculated SPHI was considered as the mid-value estimation for reserve calculations P50, dubbed PHI50. The cases for worst and bast case, P10 and P90, were estimated from percentiles.

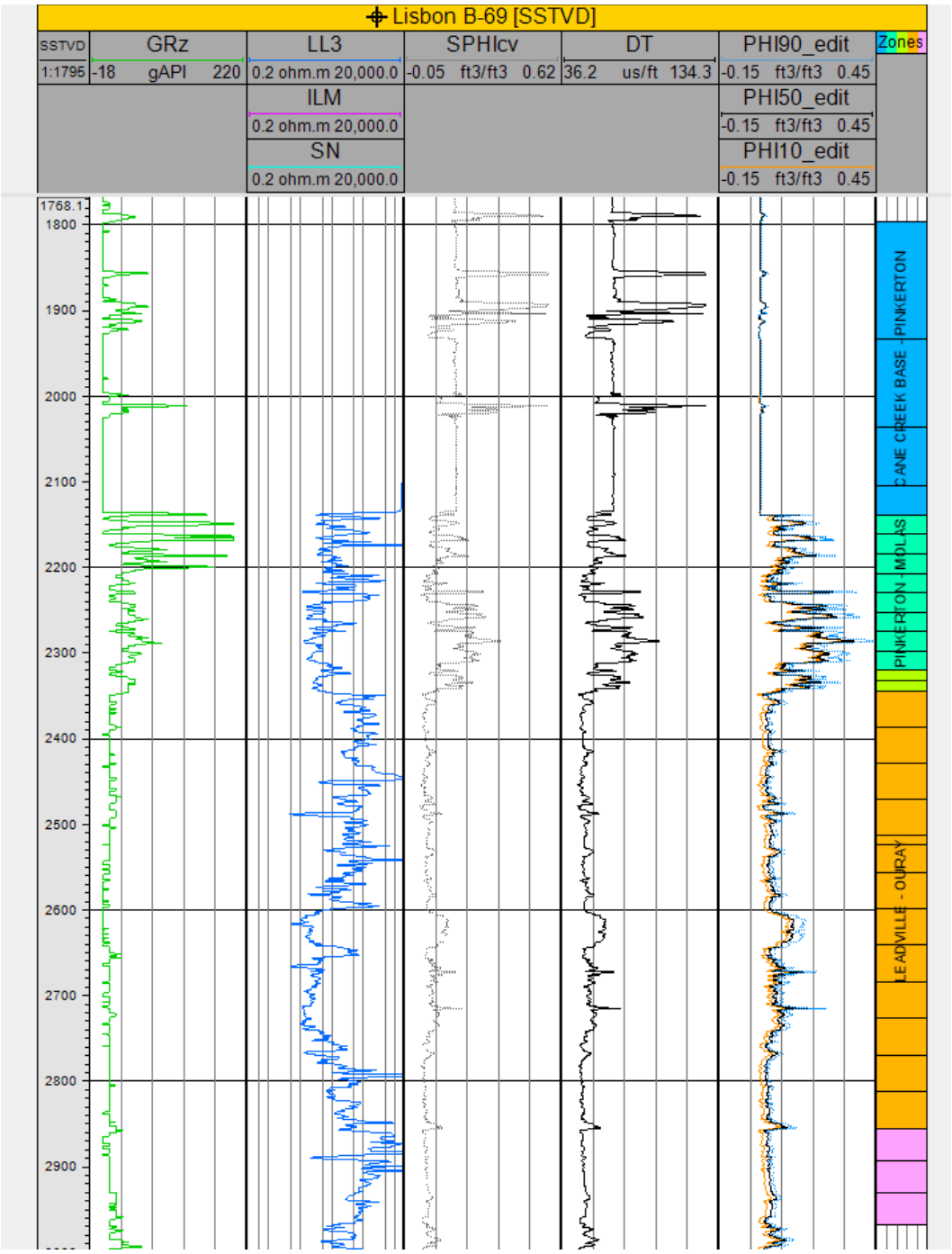

Figure 7: Petrophysical logs in the Lisbon B-69 well.

3.2 - Reservoir Modeling

The Mississippian Leadville Limestone is the primary target for the Lisbon AGI project. To assess the viability of using this formation for the injection of acid gas from the Lisbon Gas Processing Plant, a 3D geological model of the area was built using Petrel version 2024.4. Then, using Schlumberger's simulation software, Eclipse Compositional E300 (version 2021.2), a suite of reservoir simulations was executed to delineate the Maximum Monitoring Area (MMA) and Active Monitoring Area (AMA).

Geological Modeling

Geological Structural Model Development

A geological structural model was constructed using data from 150 wells with recorded formation tops within the area of interest and data from a Utah Geological Survey (UGS) publication. Of these wells, 84 have Leadville Formation tops, the target injection horizon. Surfaces were mapped from the Elbert Formation at the base to the Navajo Sandstone at the surface using these formation tops. A detailed fault model was extrapolated based on published data from the UGS report on the Mississippian Leadville Limestone by Chidsey (2008). This report served as a primary reference for structural interpretation of these critical faults, including a significant southeast-northwest trending graben observed in formations below the Paradox. Additionally, a set of northeast-southwest trending faults forms an anticline, which terminates against the graben and die out to the west of the Lisbon Field. All these faults including the major graben terminates in the base of the overlying Paradox Formation. According to the UGS report (Chidsey, 2008), this anticline acts as a trapping mechanism for hydrocarbons, leading to the development of the Lisbon Field. Figure 8 highlights the locations of the UGS cross-section (Figure 9) and surface geology in the area of interest encompassing the Lisbon Field. The basement fault network, Leadville Formation surface, and 84 wells with formation tops are shown in Figure 10.

Within the Lisbon Field, the original water-oil contact is recorded at 2570 ft below mean sea level (msl), and the gas-oil contact is at 1800 ft below msl in the Pinkerton, Molas, and Leadville Formations. Although the UGS cross-section (Figure 9) only delineates the Leadville Limestone and the overlying Paradox Formation, the tops of the Pinkerton and Molas Formations were identified from well data.

To get accurate formation surfaces above the Paradox Formation, the Lisbon Valley fault was modeled faulting the formations from the top of the Paradox to Navajo Sandstone using surface fault expression delineated by the UGS (Chidsey, 2008). This work was critical to get formation depths for the subsequent National Risk Assessment Partnership (NRAP) leakage assessment work.

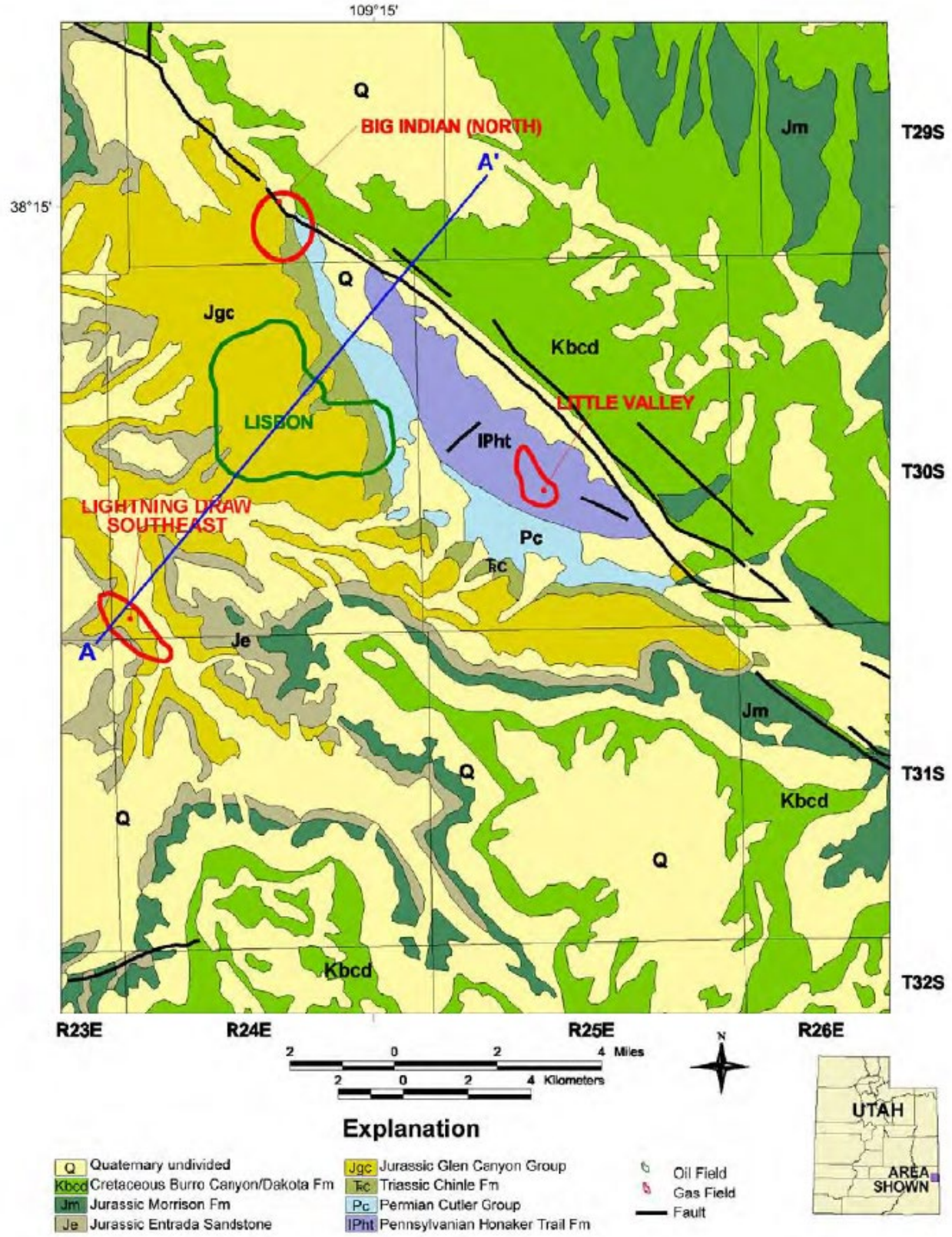

Figure 8: Surface geology of the Lisbon Field area showing the Lisbon Valley anticline and the surface expression of the Lisbon Valley fault. The cross-section in Figure 9 is indicated by A-A' (Chidsey, 2008).

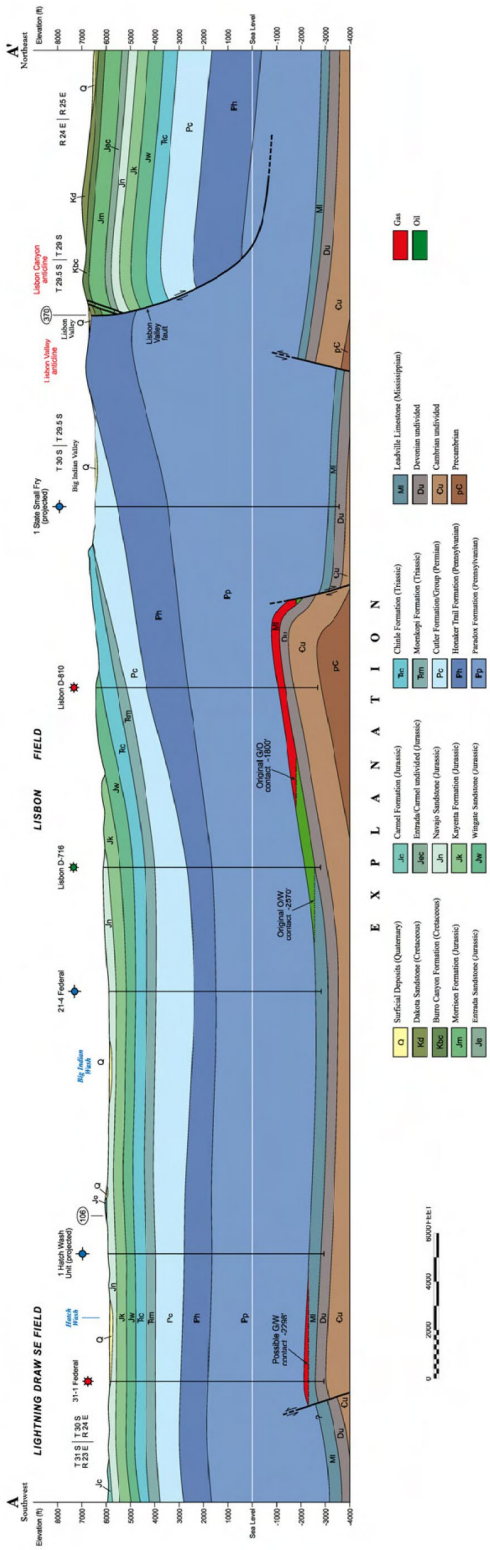

Figure 9: Cross-section through the Lisbon Field showing the major formations and faults along with the fluid contact elevations in the Leadville Limestone. This corresponds to the line A-A' in Figure 8 (Chidsey, 2008).

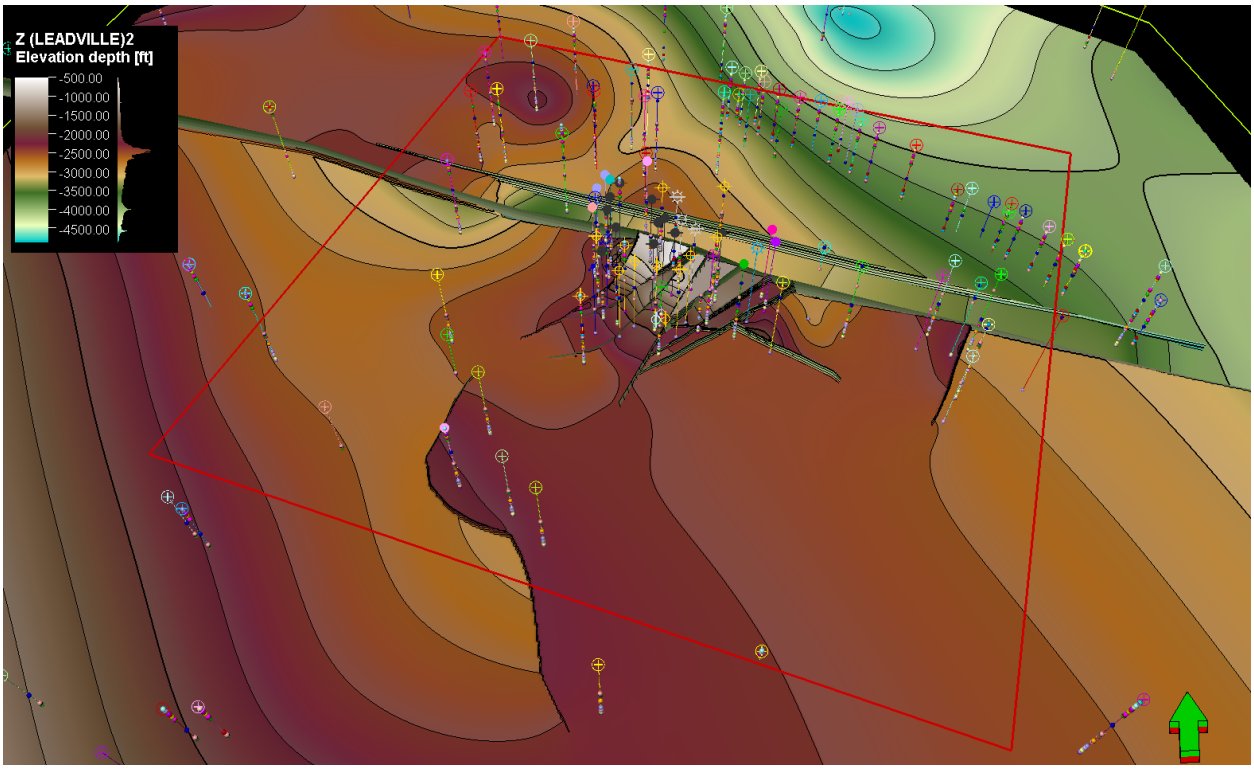

Figure 10: Wells with formation tops used in the surface modeling along with the Leadville surface showing the major southeast-northwest trending graben and the northeast-southwest trending faults that form the Lisbon Field anticline.

Simulation Model Setup

For the simulation model, the surfaces delineated in the geologic structural model for the Base of Cane Creek, Pinkerton, Molas, Leadville, Ouray, and Elbert Formations were used. The Paradox Formation serves as a sealing unit for the Pinkerton, Molas, and Leadville Limestone Formations in the Lisbon Field. It averages 4300 ft in thickness within the model boundary, composed of alternating salt and clastic layers that overlay the injection reservoir, making it an ideal sealing formation. The Base of Cane Creek was chosen as the top of the primary sealing formation in the simulation model due to its location in the bottom portion of the Paradox Formation, ensuring adequate sealing properties and optimizing computational efficiency. The cross-section in Figure 14 illustrates the reservoir and sealing configuration of the simulation model by highlighting the porosity distribution.

The model grid was discretized into 121 x 119 x 29 cells, creating a total of 417,465 active cells. To align the model with the southeast-northwest trending graben, the grid was rotated by 22 degrees. The cell dimensions are approximately 150 m x 150 m, resulting in a surface area of about 22,500 square meters per cell. The fault model was incorporated into the simulation grid, forming an unstructured pillar grid. Grid trends were controlled to avoid skewed cells and to accurately represent the fault architecture.

Dynamic Modeling

A dynamic numerical model was developed to simulate the plume movement and structural trapping of AGI in the depleted oil and gas reservoirs of the Pinkerton, Molas, and Leadville Limestone Formations. The model captures the interactions of these fluids with the reservoir, providing insights into long-term reservoir behavior and fluid migration.

Porosity and Permeability Estimation from Well Logs

The porosity of the formations was estimated using data from 32 wells, employing density and neutron porosity logs. These logs were processed using industry-standard correlations to estimate porosity values across the reservoir. The detailed development of P10, P50, and P90 porosity estimates is covered in section 3.1 – Petrophysical Description. However, modifications were required for the Paradox Formation, where the presence of salt caused standard porosity correlations to overestimate the porosity. The porosity in these sections was reduced by an order of magnitude to account for the impact of salt.

Permeability was calculated using the Kozeny-Carman equation, which correlates porosity with permeability, following industry-standard practices. Figure 11 presents well logs that illustrate the estimated P10, P50, and P90 porosity and permeability values. These estimates were crucial for constructing the dynamic simulation model.

Property Population Across the Dynamic Model Domain

The estimated porosity and permeability values from the well logs were then populated across the entire reservoir domain. To achieve this, data analysis tools were used to create semi-variograms, define correlation lengths, and establish trend azimuths for each geological formation. This statistical analysis helped generate probability distributions for porosity, which were used to guide the spatial population of porosity in the model.

A sequential gaussian simulation (SGS) was then used to distribute porosity values across the dynamic model domain. Three porosity distributions—P10, P50, and P90—were created to reflect a range of possible reservoir conditions. Figure 12 shows the resulting porosity distributions at the top of the Leadville Limestone.

Permeability was then calculated using the Kozeny-Carman equation, applying the same parameters used in the well log analysis. This approach eliminated potential uncertainties that could arise from using sequential gaussian simulation to populate upscaled permeability values calculated in the well logs. Figure 13 shows the P50 permeability distribution at the top of the Leadville Limestone in the left panel and the P10 and P90 distributions in the smaller panels on the right.

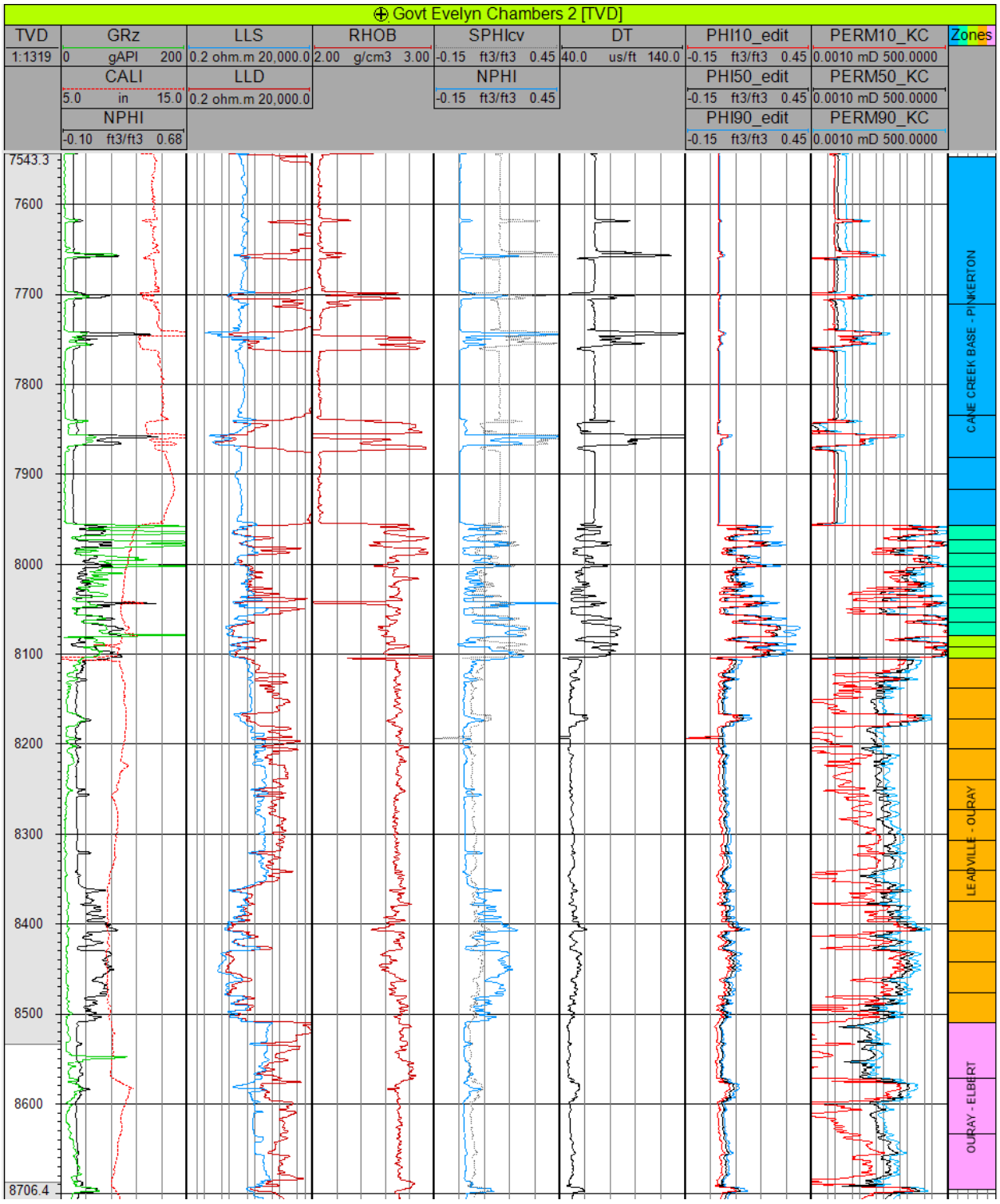

Figure 11: Example of the input well logs from the Govt Evelyn Chambers 1 well along with the derived porosity and permeability logs.

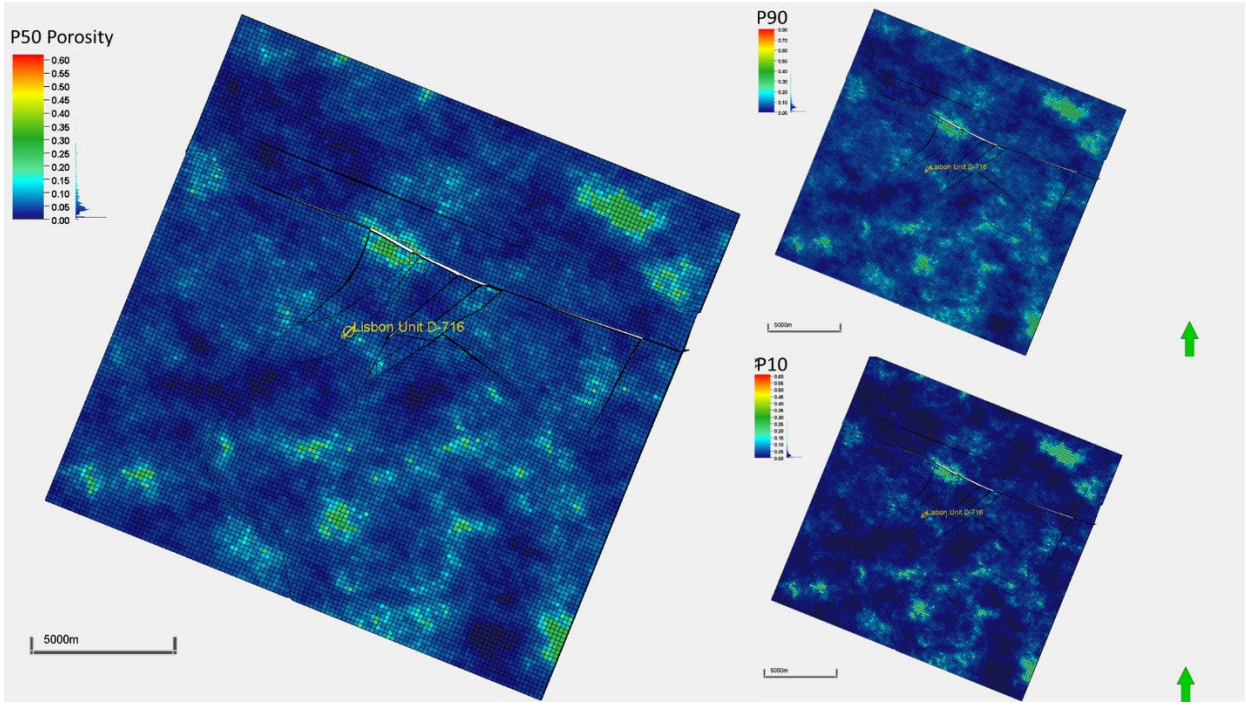

Figure 12: The P10, P50, and P90 porosity distribution at the top of the Leadville Limestone. The P50 is highlighted in the bigger panel on the left.

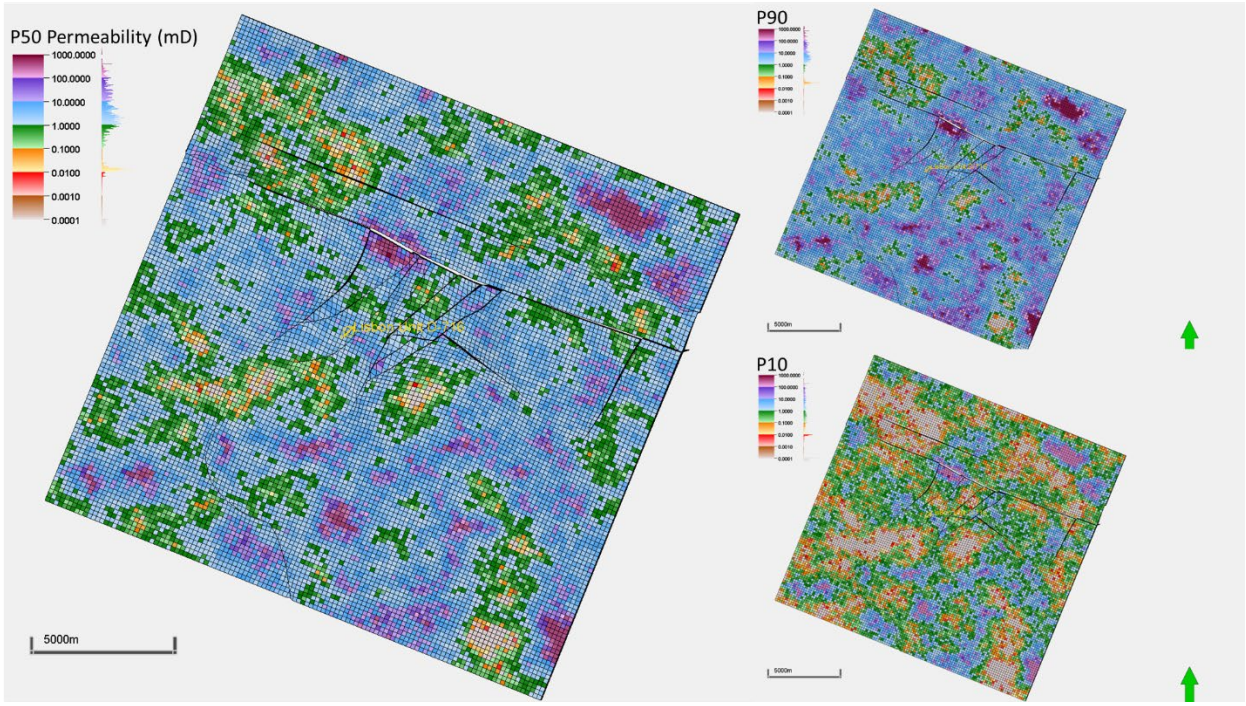

Figure 13: The P10, P50, and P90 permeability distribution at the top of the Leadville Limestone. The P50 is highlighted in the bigger panel on the left.

Reservoir Fluid Model

The reservoir fluid model was developed using legacy data from well files and information provided by the field operator. In-situ water salinity was set to 56,206 ppm total dissolved solids, based on data from well files and operator input. The oil composition was modeled using hydrocarbon analysis data from three wells, Lisbon U D-610 (1988–1989), Lisbon B-912 (1961), and Cordillera St 1 (1978), with the hydrocarbon compositions listed in Table 2. Due to no recent compositional fluid data being available, the reservoir fluids were assumed to consist of 5% gas and 95% water in the gas cap, 30% oil and 70% water in the oil zone, and brine below the oil-water contact.

The reservoir gas cap prior to injection contained 0.053% H_2S and 0.8% CO_2. Fluid contacts, based on data from the UGS, place the gas-oil contact at -1800 ft msl and the oil-water contact at -2570 ft msl (Figure 14) (Chidsey, 2008).

Table 2: Hydrocarbon composition used in the simulation based on legacy well data in three nearby wells within the Lisbon Field.

Species		Gas Cap (%)	Oil Region (%)
Hydrogen Sulfide	H_2S	**1.05**	**0**
Carbon Dioxide	CO_2	**15.94**	**0.11**
Nitrogen	N_2	**11.36**	**0.04**
Methane	C_1	**62.92**	**0.71**
Ethane	C_2	**5.07**	**0.81**
Propane	C_3	**2.16**	**1.81**
iso-Butane	IC_4	**0.36**	**0.62**
n-Butane	NC_4	**0.7**	**2**
iso-Pentane	IC_5	**0.18**	**1.71**
n-Pentane	NC_5	**0.17**	**3.1**
Hexanes	C_6	**0.09**	**7.23**
Heptanes	C_7+	**0**	**81.86**

Initial Conditions and Injection Schedule

The model assumes that the reservoir pressure was in hydrostatic equilibrium prior to the commencement of historical AGI starting on June 1, 2015. However, the absence of reliable historical injection and production data limits the accuracy of pre-2015 reservoir conditions assumption.

The primary AGI well, Lisbon Unit D-716 (API 4303731034), began injecting a mixture of 10% H_2S and 90% CO_2 in June 2015. The historical injection rate was modeled at 750 MSCF/day from June 1, 2015, until January 1, 2025. From this point forward, the injection rate was projected to increase to 12,000 MSCF/day, with injection continuing until January 1, 2055, a total injection duration of 40 years.

Produced water injection was modeled at well Lisbon C-99 (API 4303730693) from May 1, 2022, until the well was closed on October 14, 2023. Historical injection rates and schedules for Lisbon Unit D-716 and Lisbon C-99 were based on data submitted to the Department of Oil, Gas, and Mining (DOGM).

The total simulation period was 490 years, from June 1, 2015, to January 1, 2505. This extended simulation time was necessary to capture the long-term movement of the H_2S and CO_2 plumes within the reservoir. Given that the injection occurred near the base of an anticline, the plumes are expected to continue migrating up-dip for a prolonged period. This long-term simulation provides critical insights into the fate of injected gases and their potential for long-term containment in the reservoir.

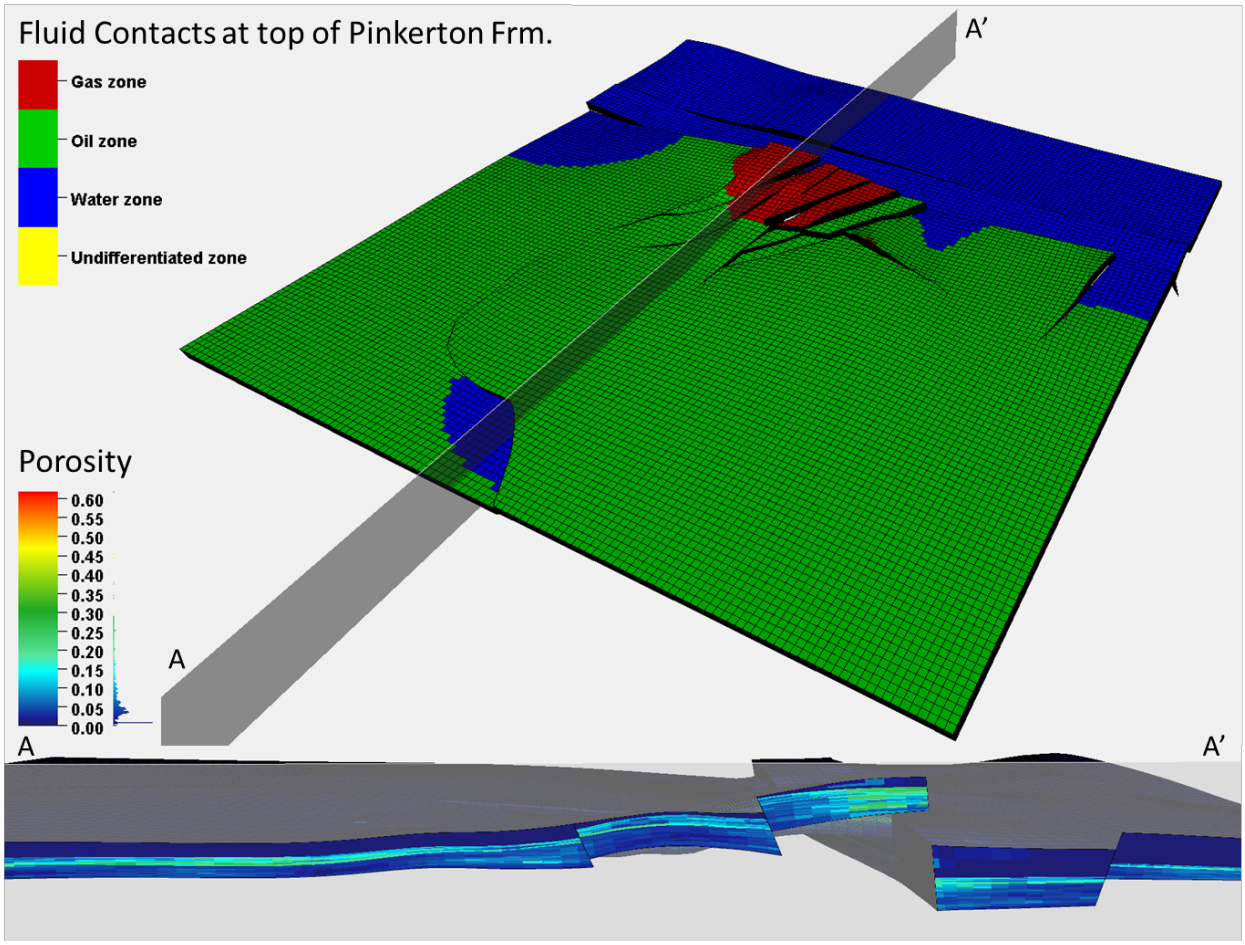

Figure 14: Simulation model grid showing the fluid contacts at the top of the Pinkerton Formation and a cross-section (A-A') highlighting the complex structure of the Lisbon Valley anticline through the injection area and the porosity distribution.

Injection Plume, Containment, and Plume Migration

A total of 7.474 million metric tons of acid gas, a 90% CO_2 and 10% H_2S mixture, was injected into the reservoir over a 40-year period. The simulations modeled the pressure behavior, plume migration, and containment within the reservoir throughout and after the injection process.

Reservoir Pressure Management

Simulation results indicate that no active pressure management is required due to the lateral continuity of the reservoir unit across the Paradox Basin, which helps dissipate pressure increases. The maximum reservoir pressure was found to be 3998 psi at the end of the injection period in the P10 scenario. In the P50

and P90 scenarios, the maximum reservoir pressures were even lower, reflecting reduced pressure buildup under more favorable porosity and permeability estimates.

At the AGI well Lisbon Unit D-716, the calculated pressure at 80% of lithostatic stress is 7376 psi. During the entire injection period, neither the bottom hole pressure nor the reservoir pressure exceeded this threshold. In the P10 scenario, the highest bottom hole pressure of 6,764 psi occurred when the injection volume increased from 750 MSCF/day to 12,000 MSCF/day on January 1, 2025. This change caused a temporary pressure spike, but the system remained below the calculated 80% of lithostatic stress limit of 7376 psi. Figure 15 illustrates the pressure profile from 2015 to 2205, capturing the critical pressure changes during and after the injection.

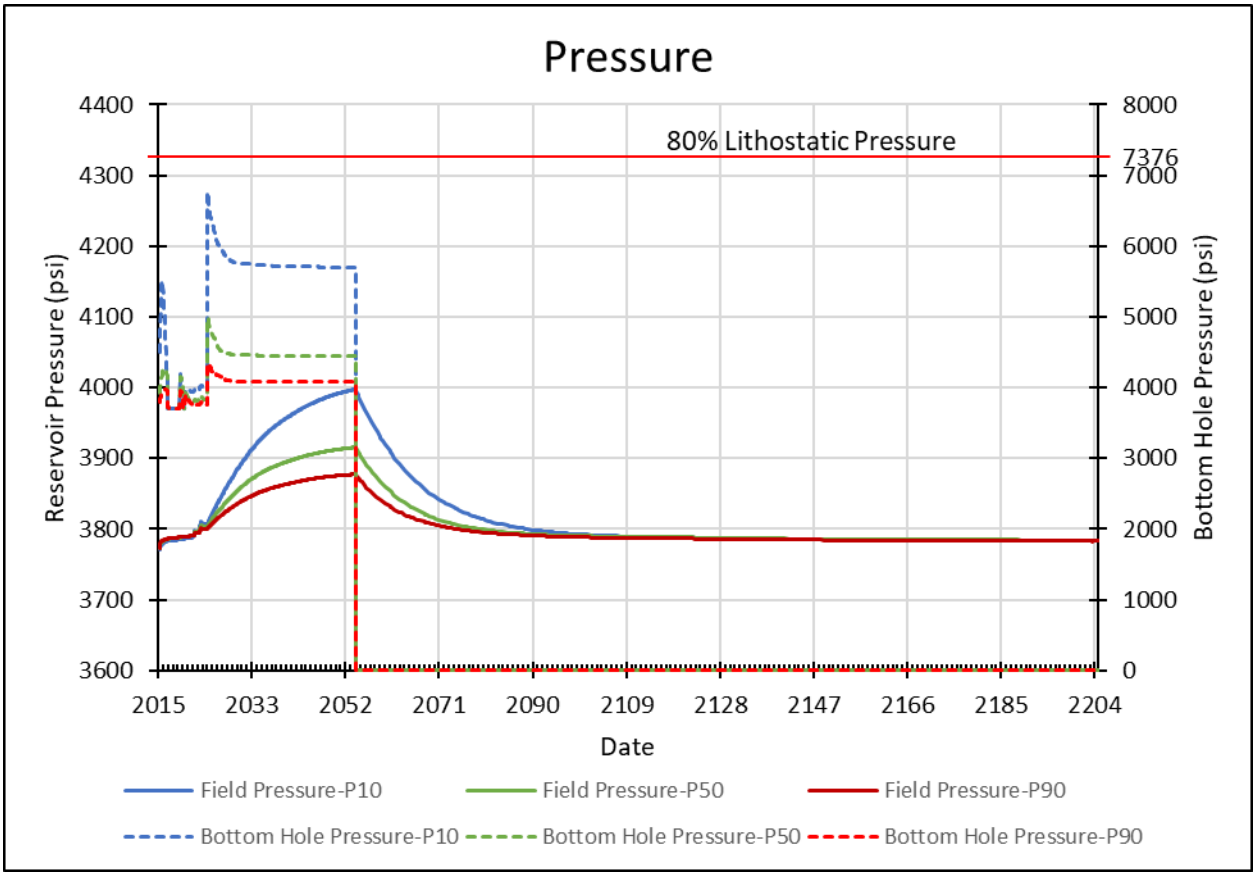

Figure 15: Reservoir pressure and bottom hole pressure at the AGI well Lisbon Unit D-716.

AGI Plume Behavior and Migration

The simulation results revealed that the CO_2 and H_2S plumes occupied the same area and followed similar migration patterns. The CO_2 plume movement over time is highlighted in Figure 16 for the P10 case, Figure 17 for the P50 case, and Figure 18 for the P90 case. The H_2S plume had lower saturation compared to the CO_2 plume but otherwise mirrored its evolution. Thus, for simplicity, only the CO_2 plume evolution is shown in Figure 16, Figure 17, Figure 18, and Figure 19, with the understanding that the H_2S plume would behave similarly and occupy the same area.

Over the 490-year simulation period, the CO_2 and H_2S plumes continued to migrate up-dip from the bottom to the top of the anticline. After 150 years, the plume's movement slowed significantly, indicating stabilization. In the P10 scenario, the plume slowed to about 23 ft/yr, while in the P50 and P90 scenarios, the plume's migration reduced to 17 ft/yr and 8 ft/yr, respectively.

In the P10 scenario, the plume eventually reached the graben fault and fully stabilized 285 years after injection ceased. For the P50 and P90 scenarios, plume movement slowed and stopped 195 years after injection once it reached the top of the anticline. At this point, no further up-dip movement was possible due to the substantial offset created by the interaction between the anticline and the graben fault.

The graben down-drop block, situated significantly lower than the anticline's peak, serves as a critical containment structure. This geological configuration prevents further migration of the plume, ensuring that no additional wells could be impacted. Moreover, all faults in the system terminate in the bottom of the Paradox Formation, eliminating the possibility of vertical migration of CO_2 or H_2S through the faults. This effectively prevents any interaction with shallow groundwater or any risk of surface leakage, as shown in Figure 9 and Figure 19.

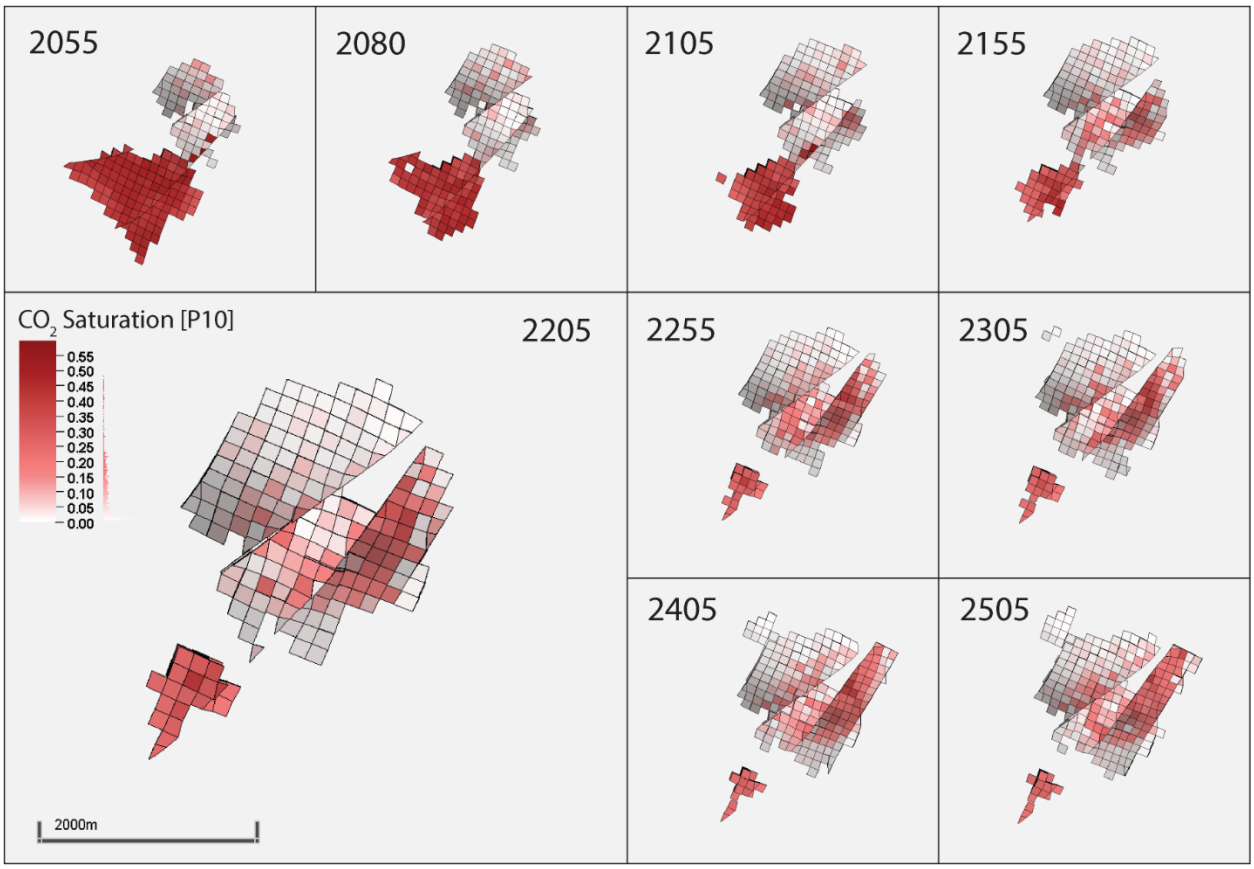

Figure 16: P10 CO_2 saturation evolution through time highlighting the plume stabilization at 150 years post-injection in the large panel at year 2205.

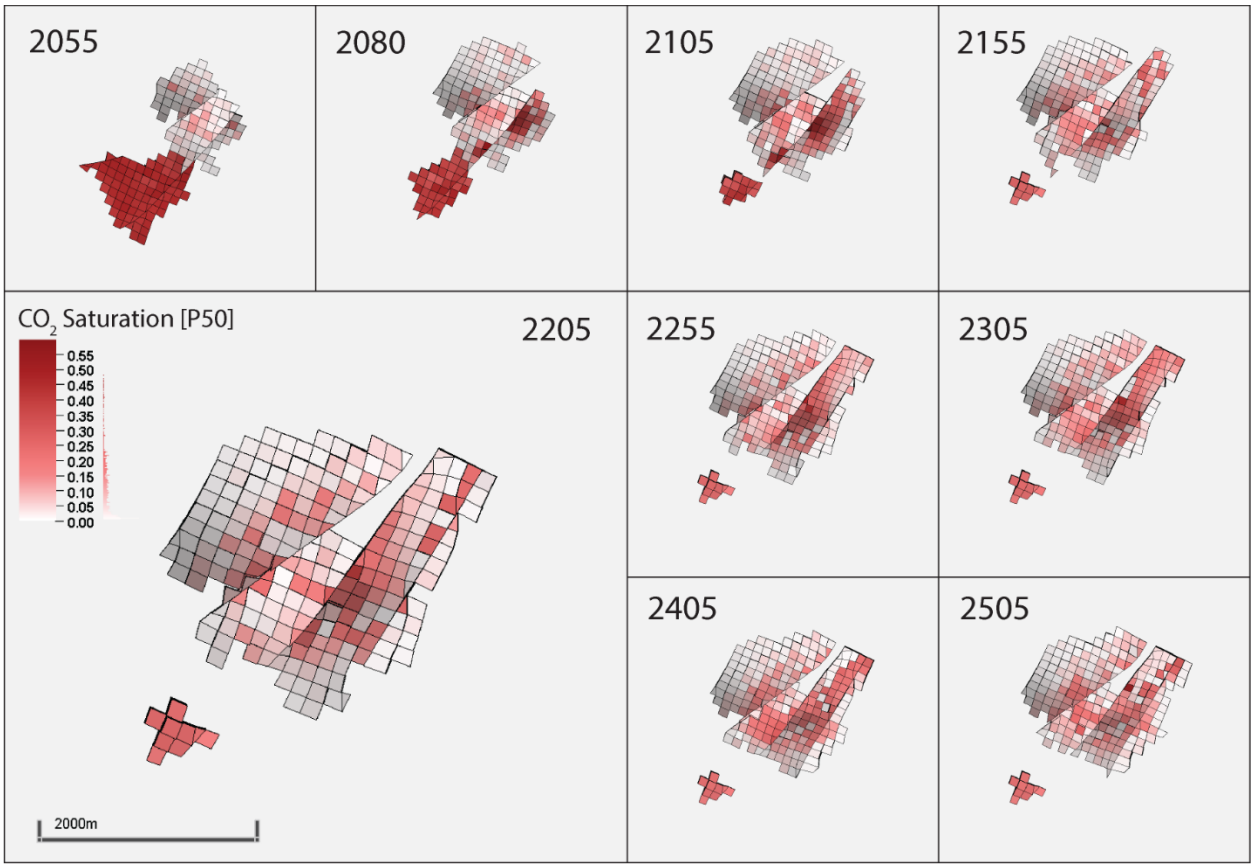

Figure 17: P50 CO_2 saturation evolution through time highlighting the plume stabilization at 150 years post-injection in the large panel at year 2205.

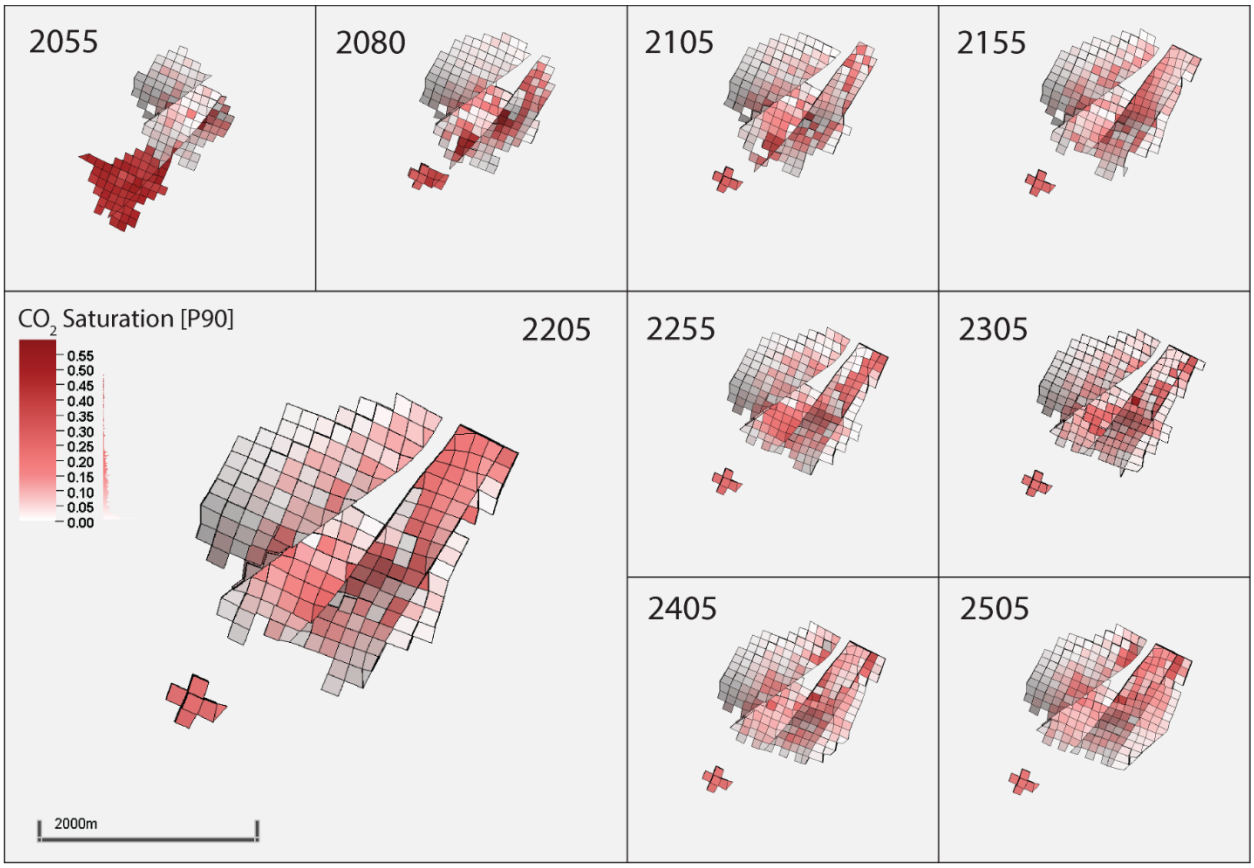

Figure 18: P90 CO_2 saturation evolution through time highlighting the plume stabilization at 150 years post-injection in the large panel at year 2205.

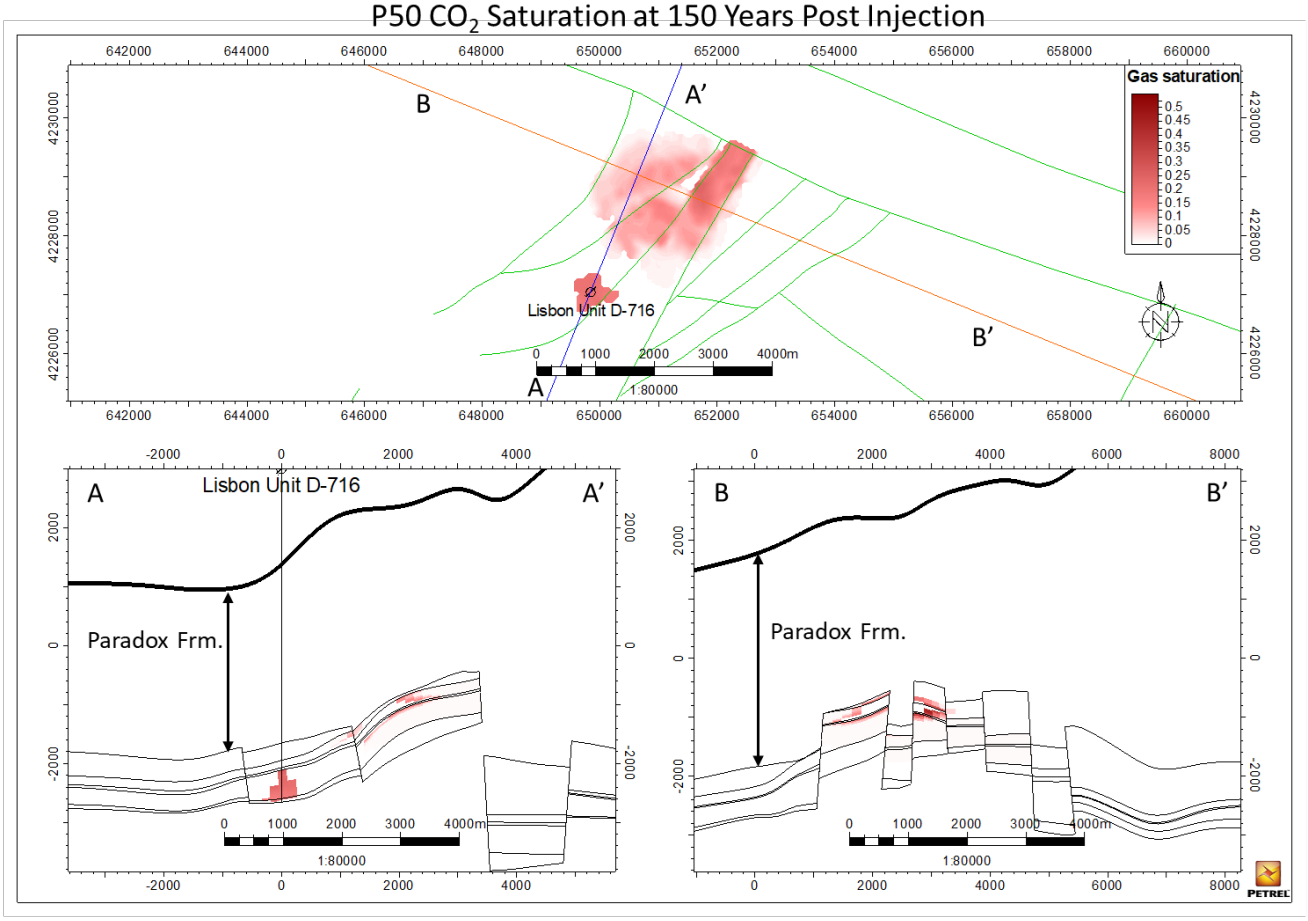

Figure 19: P50 CO_2 saturation profile and cross-sections through the Lisbon Field. Panel A-A' highlights the geometry of the top of the anticline and graben down-drop block.

Plume Area Stabilization

The simulation demonstrates that the CO_2 plume area stabilizes approximately 10 years after injection ceases, highlighted in Figure 20, although it continues to move up-dip until stabilizing against the top of the anticline in 2205. Beyond this point, the plume area only increases by 20% to 26% over the remaining 445 years of the simulation, corresponding to an annual increase in plume area of around 0.05% after 2060. This indicates a rapid stabilization in the rate of plume growth shortly after injection stops, even as the plume continues its slow up-dip migration. Ultimately, the plume reaches the graben fault at the top of the anticline, where its movement ceases entirely due to the geological constraints of the formation.

Overall, the simulation results demonstrate that the injected CO_2 and H_2S are effectively contained within the reservoir. The combination of geological features such as the anticline and graben fault, along with the termination of faults in the base of the Paradox Formation, provide barriers to plume migration. The long-term stabilization of the plume further confirms that the injected gases will remain safely trapped within the reservoir for the foreseeable future.

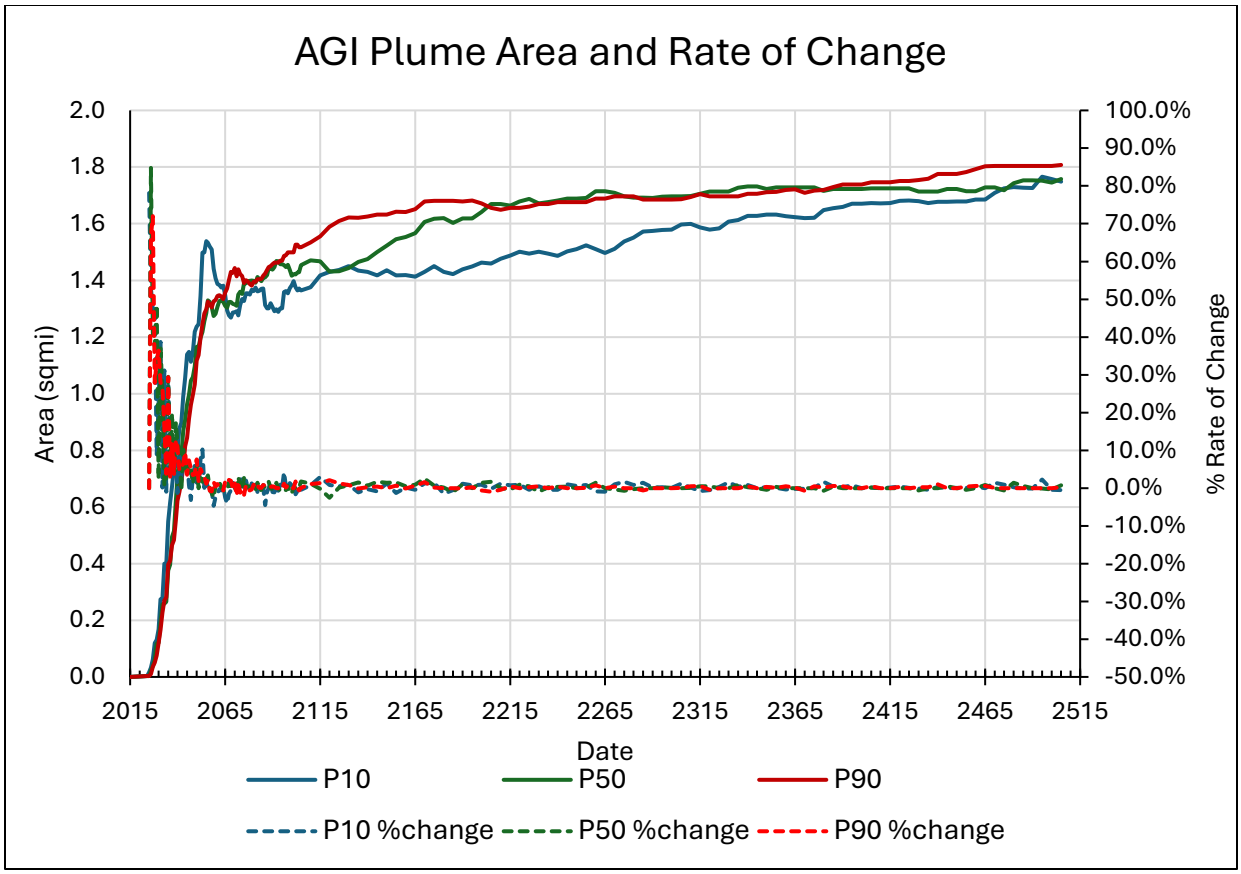

Figure 20: Area of the CO_2 plume and rate of change in plume size through time for the P10, P50, and P90 simulation cases. Plume area rate of change stabilizes around 5 years after injection stops at 2060. The plume area continues to increase slowly over the entire simulation time at a rate of about 0.05% per year post 2060.

3.3 - Delineation of the Monitoring Area and Monitoring Timeframes

Maximum Monitoring Area

Per 40 CFR 98.449, maximum monitoring area is defined as equal to or greater than the area expected to contain the free phase CO_2 plume until the CO_2 plume has stabilized plus an all-around buffer zone of at least one-half mile. The MMA is established to ensure that the monitoring region fully encapsulates any potential plume movement until it stabilizes. To determine the MMA, reservoir modeling was conducted using geological data from nearby wells, along with historical production and injection records modeled under three scenarios—P10, P50, and P90. The plume stabilization occurred in all scenarios around year 2205. At year 2205 the plume extent for each scenario was combined to estimate the maximum active CO_2 plume area, represented by the blue polygon in Figure 21. The green dashed polygon in Figure 21 represents the MMA. A list of wells within the MMA and their current statues are shown in Table 3.

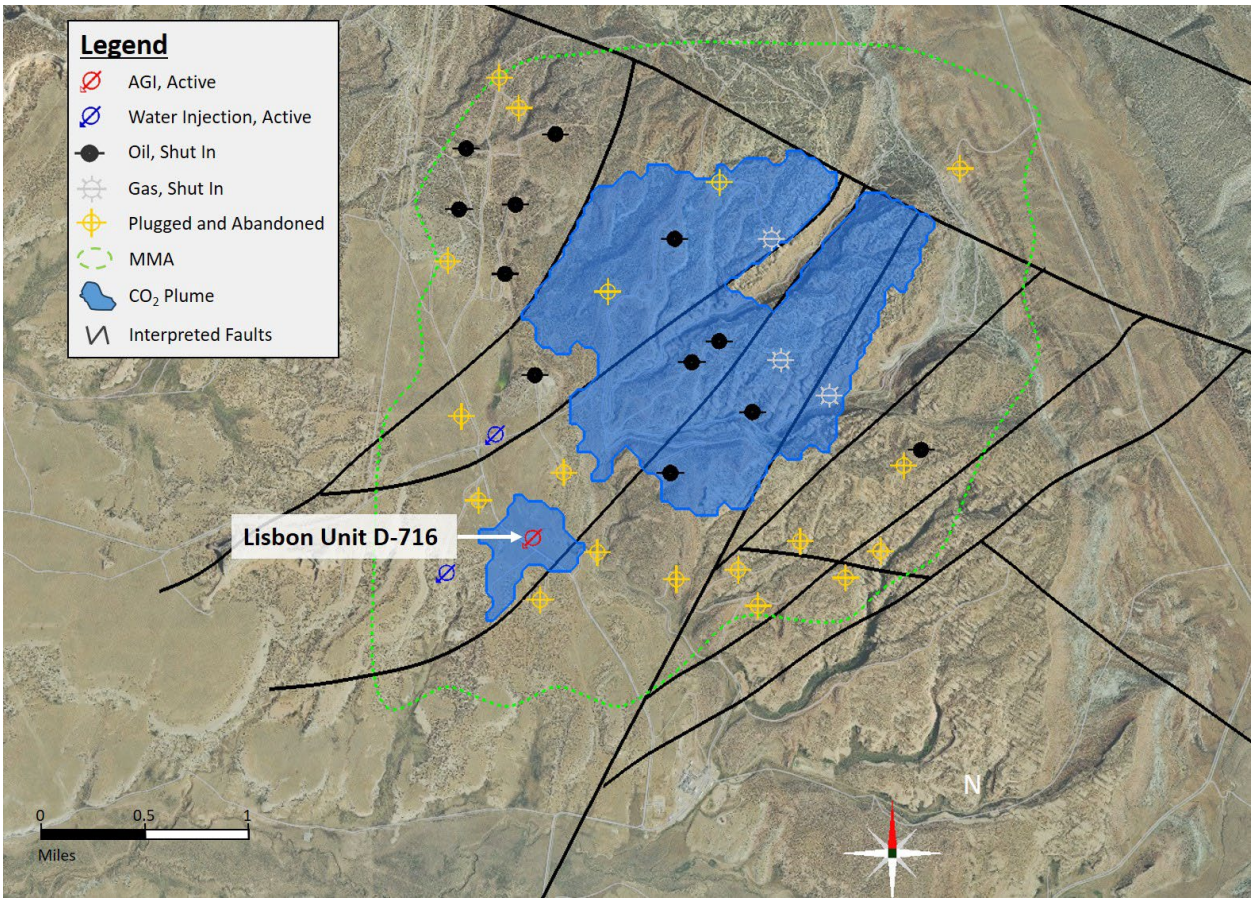

Figure 21: MMA shown in the green dashed polygon with the maximum AGI plume at 150 years post-injection shown in the blue polygon and all the wells within the MMA identified.

Table 3: List of wells that are within the MMA.

Well Name	API	Current Well Statues
Belco St 4 (Lisbon B-816)	4303716244	Water injector
Lisbon 10-33MC	4303750019	Oil producer – shut in
Lisbon A-710	4303731194	Plugged & abandoned
Lisbon A-715	4303716252	Plugged & abandoned
Lisbon A-814	4303716238	Plugged & abandoned
Lisbon B-614A	4303731351	Oil producer – shut in
Lisbon B-615	4303715123	Oil producer – shut in
Lisbon B-616	4303716242	Plugged & abandoned
Lisbon B-69	4303716241	Plugged & abandoned
Lisbon B-810	4303731433	Oil producer – shut in
Lisbon B-814	4303730082	Plugged & abandoned
Lisbon B-815	4303716243	Plugged & abandoned
Lisbon B-84	4303730054	Oil producer – shut in
Lisbon B-94	4303730695	Oil producer – shut in
Lisbon B-99	4303716239	Plugged & abandoned
Lisbon C-69	4303716245	Oil producer – shut in

Lisbon C-715	4303731074	Plugged & abandoned
Lisbon C-74	4303711341	Plugged & abandoned
Lisbon C-815	4303716249	Plugged & abandoned
Lisbon C-84	4303716246	Plugged & abandoned
Lisbon C-910	4303731323	Oil producer – shut in
Lisbon C-94	4303716247	Oil producer – shut in
Lisbon C-99	4303730693	Water injector
Lisbon D-616	4303715049	Plugged & abandoned
Lisbon D-715	4303716252	Plugged & abandoned
Lisbon D-816	4303716253	Plugged & abandoned
Lisbon D-89	4303716251	Oil producer – shut in
Lisbon U B-610	4303716469	Oil producer – shut in
Lisbon U D-610	4303730694	Gas producer – shut in
Lisbon Unit A-911	4303731014	Gas producer – shut in
Lisbon Unit D-716	4303731034	Acid gas injection
Lisbon Unit D-84	4303716250	Oil producer – shut in
NW Lisbon State A1 (C-92)	4303711342	Plugged & abandoned
NW Lisbon USA A-2 (D-810)	4303716471	Gas producer – shut in
NW Lisbon USA B-1 (B-614)	4303716468	Plugged & abandoned
NW Lisbon USA-C3 (C93)	4303716470	Plugged & abandoned

Active Monitoring Area

Per 40 CFR 98.449, active monitoring area is defined as the area that will be monitored over a specific time interval from the first year of the period (n) to the last year in the period (t). The boundary of the active monitoring area is established by superimposing two areas:

(1) The area projected to contain the free phase CO_2 plume at the end of year t, plus an all around buffer zone of one-half mile or greater if known leakage pathways extend laterally more than one-half mile.

(2) The area projected to contain the free phase CO_2 plume at the end of year t + 5.

In this analysis, the AMA is delineated after 30 years of injection and 10 years of post-injection monitoring (year 2060) with a one-half mile buffer drawn around the free phase CO_2 plume that also encompasses the area of the projected free phase CO_2 plume at year t+5 (2065). The red dashed polygon in Figure 22 shows the free phase CO_2 area plus a one-half mile buffer zone and the blue polygon shows the free phase CO_2 area in the year 2065.

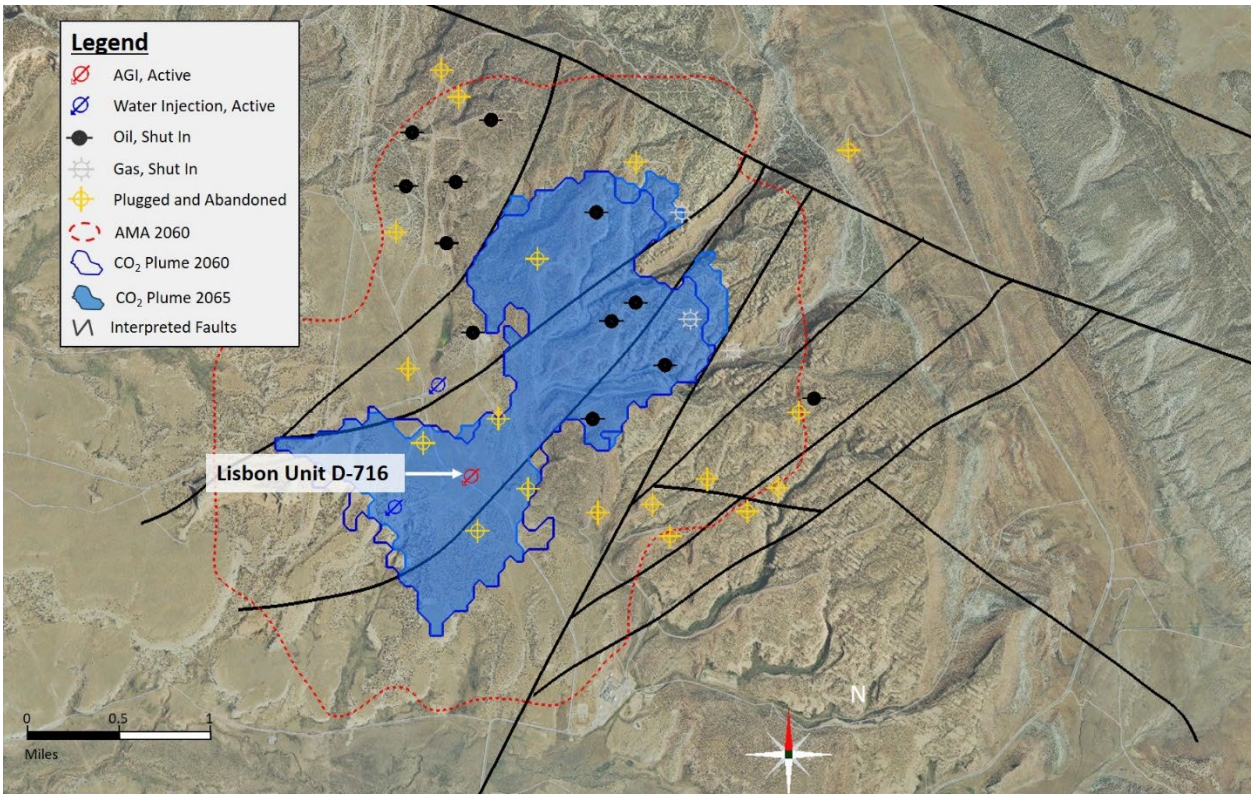

Figure 22: AMA shown in the red dashed polygon at 10 years post-injection (2060) with the maximum AGI plume at 15 years post-injection (year 2065) shown in the blue polygon.

Monitoring Timeframe

The projected monitoring timeframe extends to 150 years post-injection, based on simulation results. The geological structure of the anticline controls the movement of the CO_2 and H_2S plume, causing it to migrate up-dip throughout the entire simulation. Due to the specific geometry of the anticline and its associated graben fault, the plume can only migrate up-dip until it encounters the graben fault. Once the plume reaches the graben fault and associated down-dropped block, further up-dip movement ceases, ensuring that no additional wells will be impacted by the plume. In addition, fault terminations at the base of the Paradox Formation eliminate the risk of leakage pathways to the surface or contamination of shallow underground sources of drinking water (USDWs).

This up-dip movement begins to stabilize as early as 2115 for the P90 and P10 scenarios, and by 2140 for the P50 scenario. By the year 2200, the majority of the plume front has intersected the graben fault, with only minor up-dip movement occurring around the plume's periphery for the remainder of the simulation period. This stabilization around the year 2200 supports a year t+5 monitoring timeframe of 150 years ending at year 2205, after which continued monitoring is deemed unnecessary.

4.0 - Risk Assessment and Monitoring Strategies for Leakage Pathways

There are seven potential leakage pathway risks associated with the AGI from the Lisbon Gas Processing Plant. We identify the likelihood, timing, magnitude, and monitoring strategies associated with each pathway. The seven categories of potential leakage pathways are: surface equipment, future drilling

operations, legacy wells, seal and confining system, lateral migration, fractures and faults, and induced seismicity. We use quantitative methods for the legacy wellbores, seal and confining system, faults and fractures, and induced seismicity, and use informed qualitative descriptions for the remaining pathways.

4.1 - Surface Equipment Risks

Likelihood

Both CO_2 and H_2S are corrosive in engineered systems, which over time, creates the potential for leakage to occur. The risk of leakage due to corrosion is lessened through strict adherence to regulatory requirements and industry standards. These requirements and standards necessitate regular inspection of surface equipment. The most likely surface equipment to express a leak would be the flanges and valves in the pipelines. Although mitigative measures are in place to prevent the leakage of CO_2 into the atmosphere from surface equipment, there exists the possibility for such leakage to occur. However, given compliance with the construction and inspection strategies, the likelihood of leakage via this pathway is low. Another, albeit unlikely, possibility is the potential for an accident or natural disaster to damage the surface infrastructure, but the Lisbon Valley is situated in a relatively seismically quiescent part of the Paradox Basin, and the operational staff are trained in safety protocols.

Timing

Leakage risk via this pathway will be consistent with the operational duration of the project but can be remediated when detected.

Magnitude

If leakage is detected, the magnitude of carbon dioxide lost from the Lisbon Gas Processing Plant will be quantified using the balance of mass equations presented in section 7.0 of this MRV plan, as stipulated by 40 CFR § 98.230-238. Furthermore, the magnitude of the leak would depend on both the duration of the leak and the rate of loss of the leak.

Monitoring

GNG Energy will use several different methods of monitoring to detect leakage of CO_2 and H_2S from surface equipment. These strategies include fixed in-field and personal H_2S sensors, frequent periodic visual inspection of the equipment, especially the flanges and the valves, and continual monitoring of operational parameters, such as flow rates. The detection of CO_2 is more challenging than that of H_2S because the parts-per-million baseline in the atmosphere is higher. Therefore, the H_2S detection will be used as a proxy for CO_2 as well. The personal monitors are set to alarm and vibrate at 10 ppm. Handheld gas detection monitors are available at strategic locations around the Plant so that plant personnel can check specific areas and equipment prior to initiating maintenance or other work. The handheld gas detectors have sensors for oxygen, LEL (explosive hydrocarbon atmospheres), H2S and carbon dioxide (CO2). If one of the gas detectors sets off an alarm, it would trigger an immediate response to address and characterize the situation.

4.2 - Future Drilling Risks

Likelihood

Future wells may be drilled into the Leadville Formation, which would create a penetration in the caprock, allowing CO_2 to be released from the reservoir to the atmosphere. At present, there are no wells that are currently planned or approved to be drilled in the MMA. Indeed, the hydrocarbon reservoirs lie above the

Leadville, which means that even if a future well is drilled, it is unlikely to be drilled deeply enough to penetrate the caprock. Therefore, we acknowledge that the likelihood of future drilling creating a leakage pathway is negligible.

Timing
In the event that a leakage pathway is created by future drilling, the duration of the leak would be the time between the penetration of the caprock and the proper sealing of the well in question.

Magnitude
It is an ongoing scientific question how much carbon dioxide can be released from a leaking well, but because the likelihood of occurrence is negligible, we assume the possible magnitude of a leak is also negligible. Should leakage occur, we will be able to quantify it through downhole pressure gauges and chemical analysis of fluids produced by the penetrating wells.

Monitoring
Continued monitoring of drilling activity by DOGM and EPA will ensure that such a leakage pathway does not occur.

4.3 - Legacy Wellbore Leakage Risks

Likelihood
Wells have the potential to be pathways for fluid leakage in a CO_2 sequestration site due to defects caused by either poor well completion or subsequent damage arising from chemical reactions and thermal and/or mechanical stresses (Gasda et al. 2004). Use of downhole pressure gauges and chemical analysis of produced fluids can inform the magnitude and presence of leakage. The NRAP-Open-IAM contains several wellbore model components that estimate the impacts of the unlikely event that leakage occurs from existing penetrations to the reservoir, the injection well, and any associated monitoring wells during and after Geological Carbon Storage (GCS) operations (Lackey et al., 2019; Vasylkivska et al., 2021; NRAP, 2023). There are four major component model types in NRAP-Open-IAM:

1. **Geologic stratigraphy**. All component models that comprise the total GCS system model in NRAP-Open-IAM are dependent upon and linked to the parameters set in the geologic stratigraphy component model. The component model allows users to define parameters describing the strata of the GCS system, including the depth and thickness of the reservoir, overlying shale, and aquifer layers.
2. **A reservoir** functions as the base of any NRAP-Open-IAM system model. Reservoir component models generate arrays representing changing pressure and fluid saturation at the top of the reservoir (reservoir-cap rock interface) over the spatial domain throughout the site performance time period of interest.
3. **Leakage pathways** simulate the upward migration of CO_2 and/or brine out of the storage reservoir as a function of leakage pathway characteristics (e.g., path length and effective permeability) and the time-varying pressure and fluid saturation output at the corresponding location in the reservoir component. Multiple leakage pathway component models can be placed in an NRAP-Open-IAM model at user-specified locations within the reservoir model domain.

4. **Receptors** receive the CO_2 or brine flow rates from leakage component models as input to calculate the magnitude of leakage into receptors of concern (e.g., potable groundwater aquifers and/or the atmosphere). aquifer receptor component models calculate the volume of groundwater in the aquifer impacted over time by leakage and account for important hydrologic and geochemical interactions as a function of user-defined groundwater aquifer characteristics. The atmospheric receptor component model calculates CO_2 dispersion in the atmosphere from one or more CO_2 leakage sources.

We used a multisegmented wellbore (MSW) model to complete the simulation, which contains geologic stratigraphy, Lookup Table reservoir component (reservoir) and multisegmented wellbore (leakage pathways).

We set seven aquifers and seven shales on the top of the reservoir. This Lookup Table reservoir component model utilizes lookup tables from outputs created with ECLIPSE (pressure and saturation from section 3.2). Gas saturation consisted of 90% CO_2 - 10% H_2S. The total water volume of storage reservoir is 3, 429, 813, 216 m^3. Table X lists the total injection amount of two gases. Using this data, we can calculate the partial pressure of two gases in P10, P50 and P90 (Eq.1) and calculate the solubility of two gases in P10, P50 and P90 (Eq.2). Two gases solubility are similar in P10, P50 and P90. Finally, the total amount of CO_2 dissolved in water is 1,468,268,740 m^3, and the total amount of H_2S dissolved in water is 70,726,178 m^3. The total injection amounts for the three cases are shown in Table 4.

$$P = nRT/V \qquad \text{Eq.1}$$

Where P is absolute pressure (Pa), V is volume (m^3), n is the number of moles of the gas present and R is universal gas constant which equals 8.3145 J/mol K.

$$c = \frac{P}{K_H} \qquad \text{Eq.2}$$

Where P is partial pressure of gases (Pa), K_H is the Henry's law constant of the gas, and c denotes the concentration of the dissolved gas.

Table 4: The total injection amount of two gases (90% CO_2 - 10% H_2S) and its final solubility in P10, P50 and P90.

The total injection numbers	Amount	Units	Amount	Units	Partial pressure (Pa) (Eq.1)	Kh ($mol/(m^3 \cdot Pa)$)	Solubility (Eq.2)
GasP10	1.03E+11	ft^3	2925482458	m^3			
H_2SP10	9.77E+06	ft^3	12348403.4	Mol	13.74726296	0.0015	0.020621
CO_2P10	8.79E+07	ft^3	111132932	Mol	123.7253686	0.00346	0.42809
GasP50	1.45E+11	ft^3	4112128997	m^3			
H_2SP50	1.37E+07	ft^3	17356793.7	Mol	13.74726338	0.0015	0.020621
CO_2P50	1.24E+08	ft^3	156211145	Mol	123.7253719	0.00346	0.42809
GasP90	2.21E+11	ft^3	6257142002	m^3			
H_2Sp50	2.09E+07	ft^3	26410631.7	Mol	13.74726357	0.0015	0.020621
CO_2P90	1.88E+08	ft^3	237695683	Mol	123.7253712	0.00346	0.42809

Lookup tables provide a means for fast calculation of reservoir response (in contrast to the full-physics numerical models from which they are derived). Based on real field data, a total of 220 wells were identified to be present at the site and used for developing the reservoir numerical model. 35 of these wells penetrate the proposed storage reservoir and aquifers were included in leakage risk assessment based on their location, depth, well radius and physical properties.

Model setup and simulation

NRAP-Open-IAM models are created by assembling a set of component models into a GCS system that best represents the GCS site of interest. The NRAP-Open-IAM models of potential subsurface gases (90% CO_2 - 10% H_2S) and brine leakage were built to estimate changes to overlying aquifers due to hypothetical leakage through potential leaking wellbores. The potential leaking wellbores contain water injector well, oil or gas producer (shut in) well and plugged & abandoned well. Figure 23(a) shows the conceptual diagram of the study area's geologic formations.

Shales are characterized by very low porosity (typically less than 5%) and very low permeability (typically less than 3.56 mD) (Goral, 2020; Shi, 2021). Based on real field data, the formations are divided into seven aquifers and seven shales in this model (Figure 23(b)). It is worth noting that the permeability of the Cane Creek is 1~10 mD, so it qualifies as an aquifer in the NRAP model. The Moenkopi and Chinle are classified as seals.

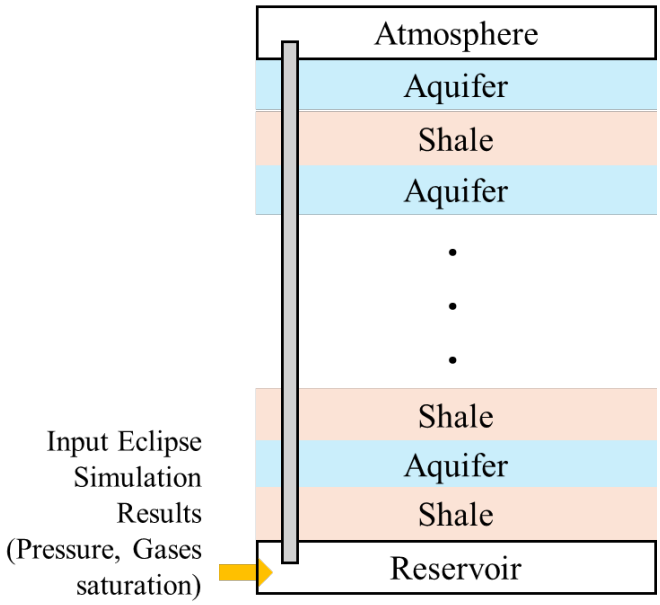

(a) Conceptual diagram

Real field data						NRAP-Open-IAM input		
Stratigraphy at Lisbon B-616		Formation Top	D (m) to Formation T	Thickness (m)	Permeability (mD)	Layer Name	Permeability (mD)	Thickness (m)
Jurassic	Glen Canyon Group	Navajo	4.19	48.70	539	aquifer7	248~539	261.68
		Kayenta	52.89	158.36	178			
		Wingate	211.26	54.61	248			
Triassic		Chinle	265.87	172.80	19	shale7	15.2~22.8	172.80
		Shinarump	438.67	22.23	124	aquifer6	99.2~148.8	22.23
		Moenkopi	460.90	91.67	16	shale6	12.8~19.2	91.67
Permian	Cutler	White Rim	not present at site			aquifer5	78~146	969.36
		Organic Rock	not present at site					
		Cedar Mesa	552.57	512.55	146			
		Elephant Canyon	not present at site					
ennsylvani	Honaker Trail	Honaker Trail	1065.12	289.04	83			
		La Sal	1354.16	79.18	78			
		Hatch	1433.34	88.58	133			
	Paradox	Ismay (A)	1521.93	28.05	0.0031	shale5	0.0031~0.0090	60.42
		Hovenweep	1549.98	32.38	0.0090			
		Gothic (B)	1582.35	40.57	30.4	aquifer4	24.32~36.48	40.57
		Desert_Creek	1622.92	30.43	0.0126	shale4	0.01008~0.01512	30.43
		Chimney_Rock	1653.34	19.50	19.5	aquifer3	15.6~23.4	19.50
		Akah	1672.85	226.63	0.0100	shale3	0.0100~0.0184	664.68
		Barker_Creek	1899.48	331.95	0.0184			
		Alkali_Gulch	2231.42	106.10	0.0109			
		Cane_Creek	2337.52	68.26	1.3	aquifer2	0.96~1.44	68.26
		Cane Creek Base	2405.78	99.08	0.0173	shale2	0.01384~0.02076	99.08
	Pinkerton	Pinkerton	2504.86	27.69	42	aquifer1	10~112	141.59
Mississipian		Molas	2532.56	18.33	112			
		Leadville	2550.89	95.57	10			
Devonian		Ouray	2646.46	16.38	2.4	shale1	1.92~2.88	16.38
		Elbert	2662.84					
	Reservoir	**Seal**	**USDW/Aquifer**					

(b) Field data and NRAP-Open-IAM input parameters

Figure 23: Conceptual diagram of the study area's geologic formations and NRAP-Open-IAM input parameters. (a) Conceptual diagram, (b) Real field data and NRAP-Open-IAM input parameters.

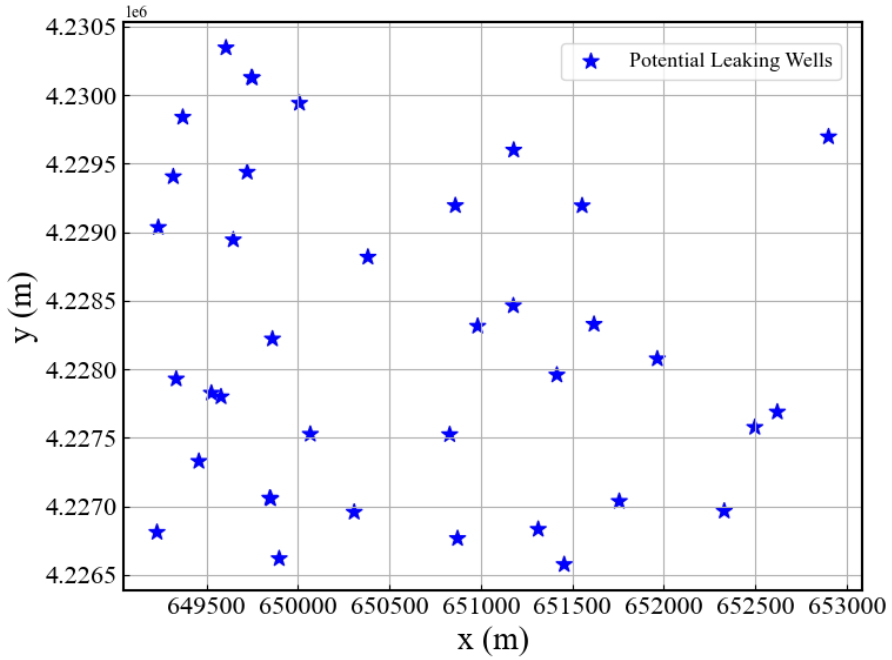

Figure 24: Description of Well locations. Blue stars represent the potential leaking wells set in NRAP Open-IMA. They are different types of wells, which include water injection wells, oil or gas production (shut in) wells and plugged & abandoned wells.

The simulation results of gas saturation and pressure in the bottom layer of the acid gas injection reservoir was used for leakage risk assessment through wellbores defined in the NRAP-leakage model (Figure 24). Pressure and gas (90% CO_2 - 10% H_2S) saturation were at yearly timesteps from 2016 until the end of injection in 2054 and then every 5 years until the MMA time is reached (2205).

Results

LHS (Latin Hypercube Sampling) is the analysis type used for stochastic simulations with random variations in parameter values. We use Latin Hypercube Sampling (LHS) analysis type with 1000 risk assessment realizations. In the simulation, the variable parameters are the thickness and permeability of the aquifers and shales.

The result showed that no well was at risk of leakage. The likelihood of leaking into the atmosphere, aquifers and into the overlying shallow USDW is virtually zero, with the 10^{th}, 50^{th} (median), and 90^{th} percentile all 0's (Figure 25).

The total gas injection is 7.47×10^9 kg. The maximum amount of gases (90% CO_2 - 10% H_2S) leakage into the aquifer from 2016 to 2206 is 0 kg among the 1000 risk assessment realizations. In conclusion, we can consider that the leakage risk through wellbores is very low.

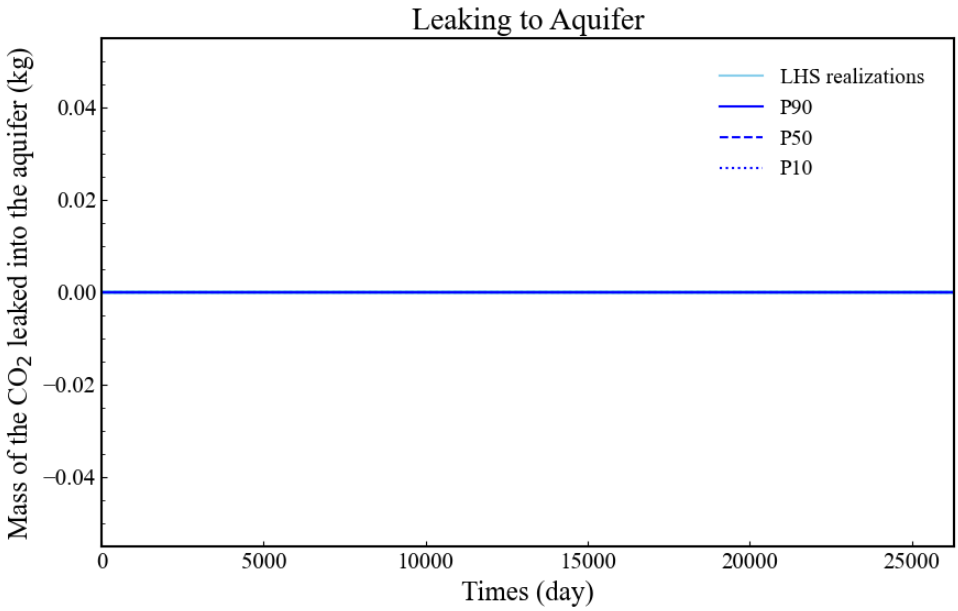

Figure 25: Leakage of CO_2 to the aquifers from all 1000 realizations for simulation. Thick lines are percentiles: P90 (solid line), P50(dash line), and P10 (dot). The leakage was numerically zero for all of the simulations.

Timing

In the event that a leakage pathway occurs from an existing well, the duration of the leak would be the time between the migration of carbon dioxide to the well and the proper sealing of the well in question.

Magnitude
It is an open scientific question how much carbon dioxide can be released from a leaking well, but because the likelihood of occurrence is negligible, we assume the possible magnitude of a leak is also negligible.

Monitoring
Described in section 5.0, we will use a variety of techniques, such as soil flux collars, pressure gauges, H_2S sensors, and monitoring of fluids from wells within the MMA to detect and quantify any leaks through existing wellbores. If any of these techniques indicate that a leak has occurred, GNG will take actions to quantify the leak based on operating conditions at the time of the detection including pressure, flowrate, and duration.

4.4 - Seal and Confining System Risks

Likelihood
The primary sealing formation for the reservoir is the Paradox Formation, a thick sequence of alternating salt and clastic units averaging 4300 ft in thickness above the reservoir units within the boundaries of the model. Due to computational constraints, only the lower part of the Paradox Formation, specifically the area below the Cane Creek unit, was incorporated into the simulation model as described in the *Simulation Model Setup* section above.

Geological data currently available indicates no faults extend from the reservoir to any overlying units above the Paradox Formation. All mapped faults terminate within the base of the Paradox, further supporting its role as an effective seal. The Paradox Formation's alternating layers of salt and clastic units act as an impermeable barrier to fluid movement. The acid gas is therefore unable to penetrate this formation, as salt of the Paradox Formation is inherently impermeable to fluid flow.

Simulation results provide additional confidence in the sealing capability of the Paradox Formation. These simulations indicate minimal leakage into the modeled lower part of the Paradox. At the time when the AMA is delineated (year 2060), the acid gas intrusion into the seal layer is measured at only 0.04% to 0.14%. Even after 500 years, the modeled projections show that only 2.97% to 7.4% of the acid gas has intruded into the seal formation. This intrusion into the sealing layer is limited to less than 100 ft vertically, underscoring the effectiveness of the Paradox Formation as a confining system. Table 5 shows the volume of acid gas that is intruded into the seal formation of the model at the AMA data of 2060, the MMA date of 2205, and the end of the simulation at 2505.

Table 5: Volume of CO_2 and H_2S (MSCF) intruded into the lower section of the Paradox Formation, the primary seal layer at the AMA time frame (year 2060), the MMA time frame (year 2205), and the end of the simulation (year 2505).

Volume of CO2 & H2S Intruded into Caprock (MSCF)

	P10		P50		P90	
2060	164,749	0.04%	158,440	0.04%	706,219	0.14%
2205	3,107,646	0.84%	5,525,433	1.42%	12,191,486	2.75%

2505	9,777,117	2.97%	15,377,544	4.23%	30,136,940	7.40%

Timing
At no point during or after injection operations is leakage expected through the Paradox Formation. This is attributed to the significant thickness and impermeability of the salt layers within the formation, which act as barrier to fluid migration.

Magnitude
Given the effectiveness of the Paradox Formation as a confining layer, no leakage is anticipated. Consequently, the magnitude of any potential leakage is considered negligible to zero. We anticipate virtually no loss of stored carbon dioxide through the caprock.

Monitoring
To ensure ongoing integrity of the storage formations, pressure and fluid monitoring will be conducted in the Lisbon D-716 well. This monitoring consisting of but not limited to soil flux measurements will provide critical data on the movement of acid gas within the reservoir. In the highly unlikely event that leakage occurs through the Paradox Formation, the reservoir model developed in section 3.2 will be revisited and updated to evaluate the extent and magnitude of any potential leakage. This proactive approach ensures that any issues can be promptly addressed and mitigated. If changes in operating parameters or other monitoring indicate leakage of CO_2 through the confining and seal system, GNG Energy will take actions to quantify the amount of CO_2 released (section 7) and take immediate action to stop it, including shutting in the well.

4.5 - Lateral Migration Risks

Likelihood
Due to the buoyant properties of supercritical carbon dioxide, it is unlikely for the CO_2 to migrate in a direction other than up dip from the injection site. The specific geometry of our site (section 3.2) shows that the CO_2 will migrate up dip until it reaches the sealing fault in the graben of the Lisbon Field anticline, where migration will stop, and the CO_2 will accumulate. Therefore, leakage due to lateral migration is highly unlikely.

Timing
Should leakage occur from lateral migration, it will be start in the years after the commencement of injection and end when the plume fully stabilizes.

Magnitude
Leakage through this pathway is not expected to occur, and therefore, the magnitude is anticipated to be negligible. Numerical simulations could further inform the magnitudes of carbon dioxide that might be lost to this mechanism, should it occur.

Monitoring
Continuous operational monitoring of the Lisbon Unit D-716 injection well will provide an indication of the movement of the carbon dioxide plume. The monitoring techniques described in section 5.0, specifically

pressure monitoring and fluid monitoring will provide the basis upon which GNG will determine if the unlikely scenario of lateral migration leakage has occurred. In addition, soil flux monitoring will provide valuable measurements of the lateral extent of the plume. If they determine that it has, the numerical model of section 3.2 will be reassessed to understand the extent and magnitude of the leak.

4.6 - Fractures and Faults Leakage Risks

Likelihood

Prior to injection, a thorough geological characterization of the injection zone and surrounding formations was performed (see section 3.2) to understand the geology and to identify the existence and distribution of faults and fractures.

All identified faults are confined to the Paradox Unit (bottom depth of 7874 ft). There is minimal chance for them to become a potential leakage pathway because no fault directly intersects with the reservoir and the surface within the MMA. Therefore, no fault can potentially serve as conduits for surface CO_2 emission.

Our team used NRAP-Open-IAM to quantitatively predict potential fault leakage on faults identified within the MMA. We assumed that all faults are planar with a dip angle 90°. The original lengths of Fault 1, Fault 3, and Fault 4 exceeded the simulation range. The strikes and lengths of the faults were calculated based on the coordinates of the fault's starting and ending points with a model domain incorporating the extent of the MMA (Figure 26).

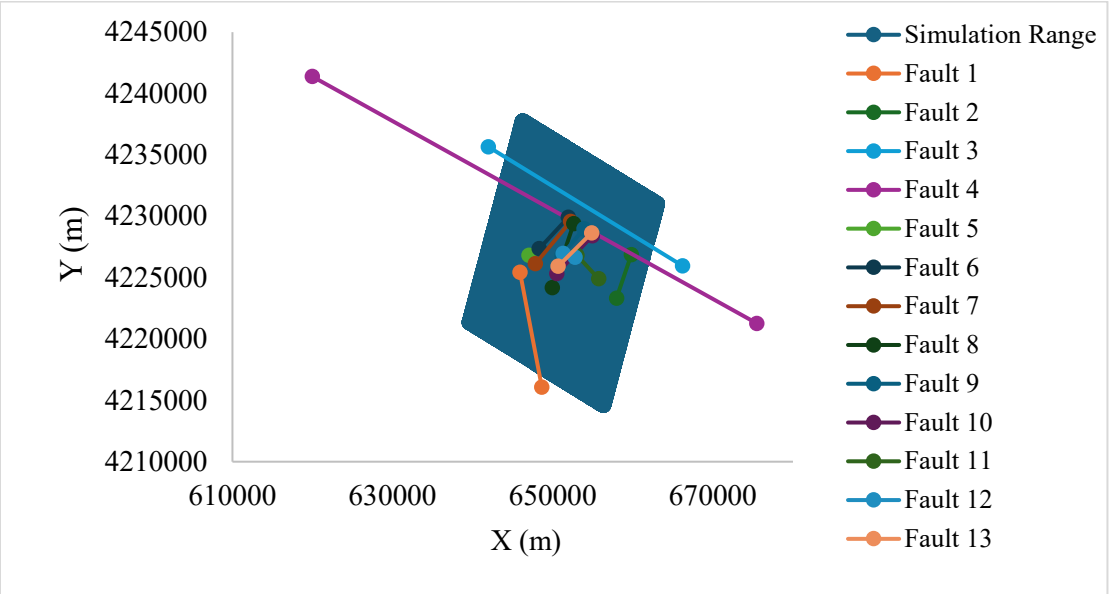

Figure 26: Fault location and simulation zone

Following the vertical fault expansions from the reservoir to the Paradox Unit, the upper aquifer that receives any potential CO_2 leakage was set to the Paradox Unit. 1000 risk assessment realizations were conducted using different distributions of the reservoir pressure and CO_2 saturations generated by the reservoir simulations, as well as a few uncertainty parameters of thicknesses of overlying formations. Pressure and gas (90% CO_2 - 10% H_2S) saturation were at yearly timesteps from 2016 until the end of

injection in 2054 and then every 5 years until the MMA time is reached (2205). Assuming a hydrostatic pressure gradient. The initial pressure of injection depth is 25.0Mpa. The average pressure at injection depth during injection is 38.32Mpa. The injection temperature is 130.56°C.

The results suggested that the likelihood of potential leakage through these faults to the Paradox Unit is zero. This also indicated that it was not possible for potential leakage to the surface through these pathways. According to the simulation result, we conclude that the CO_2 leakage rate through these faults to the overlying shallow USDW and atmosphere is zero and that the risk of leakage through this potential leakage pathway is highly improbable.

Timing

Since leakage through faults and fractures is highly unlikely, we do not anticipate this to occur during the lifetime of the project. If it does occur, the leak will last until mineralization seals permeability in the fracture.

Magnitude

The magnitude of leakage will be negligible given the highly unlikely chance that it would occur. If leakage occurs through faults and fractures, it will extend over an area and need to be quantified using surface sensors such as soil flux measurements.

Monitoring

Described in section 5.0, we will use a variety of techniques, such as soil flux collars, pressure gauges, H_2S sensors, and monitoring of fluids from wells within the MMA to detect and quantify any leaks through faults and fractures in the subsurface. Because the faults in the Leadville do not penetrate the caprock, this is a highly unlikely scenario. However, if monitoring of operational parameters and the fixed in-field gas monitors indicate possible CO_2 leakage to the surface, GNG Energy will identify which of the pathways listed in this section are responsible for the leak, including the possibility of heretofore unidentified faults or fractures within the MMA. Identifying the leakage pathway will allow Targa to take measures to quantify the mass of CO_2 emitted based on the operational conditions that existed at the time of surface emission, including pressure at the point of emission, flowrate at the point of emission, duration of the emission, and estimation of the size of the emission site. Additionally, groundwater and soil flux monitoring locations throughout the MMA will also provide an indication of CO_2 leakage to the surface.

4.7 - Induced Seismicity Risks

Likelihood

The injection of fluids into the subsurface has the ability to induce earthquakes by pressurizing the aperture of a fault, reducing the effective normal stress, and bringing the fault closer to failure in the *in-situ* stress state of the earth. Other mechanisms such as thermal stressing, poroelasticity, and Coulomb stress-transfer —the phenomenon by which stresses in the vicinity of a past rupture become perturbed—also have the ability to induce earthquakes, but these considerations are of a lesser order than the primary mechanism of the pressurization of the fault surface. Although our analysis of the induced seismicity potential of the Lisbon Field region is based predominantly on the primary mechanism, the results that we provide here are also applicable to the stability of the faults given the effects of poroelasticity and Coulomb stress-transfer. Numerical modeling would be necessary to analyze the thermal effects.

As a result of the potential to cause earthquakes from subsurface injection, it is necessary to characterize the injection site for its ability to host earthquakes. We use a three-part system that allows us to capitalize on years of research from both Stanford University and the United States National Laboratories. The first part is the assessment of historical seismicity in the region to analyze the rates of seismicity in the region of interest. The second part utilizes the work of the Stanford Center for Induced and Triggered Seismicity to assess the state of stress in the Lisbon Field region. Finally, the third segment analyzes uncertainty in the state of stress using the SoSAT tool from Nation Risk Assessment Program. These three parts will be presented in detail to illustrate that the risk of inducing earthquakes from the AGI is appreciably small. Furthermore, protocols will be suggested for the successful monitoring and maintenance of negligible induced seismicity.

Past Seismicity

An important first step in assessing the induced seismicity potential of a field site is to analyze the seismicity that has been previously recorded in the region. This gives an indication of the locations, occurrence intervals, and magnitudes to expect from the site. Figure 27 shows all earthquakes on record from the University of Utah Seismograph Stations, which is a regional network operating with a magnitude of completion of about M_w 2.5 for the region surrounding the Lisbon Field. The vertical black arrow depicts the location of the AGI, which is miles removed from any recorded seismic event. There is a cluster of events located roughly at the Lisbon Valley Mining site, which likely represents mining explosions and other activities rather than seismic rupture. Another sequence of events trends east-west along highway 90. These events had, in general, higher magnitudes that the mining-related occurrences with a maximum magnitude of M_w 3.2. It is possible that this sequence is related to the release of strain energy along a fault zone, but the sequence is more than 10 miles removed from the injection site, and there does not appear to be a connection seismically through that 10-mile region. That is, no earthquakes have been recorded between the possible fault zone and the injection site. Even considering the possible fault zone, the region is relatively seismically quiescent, which is encouraging that the injection of the acid gas is less likely to induce seismicity.

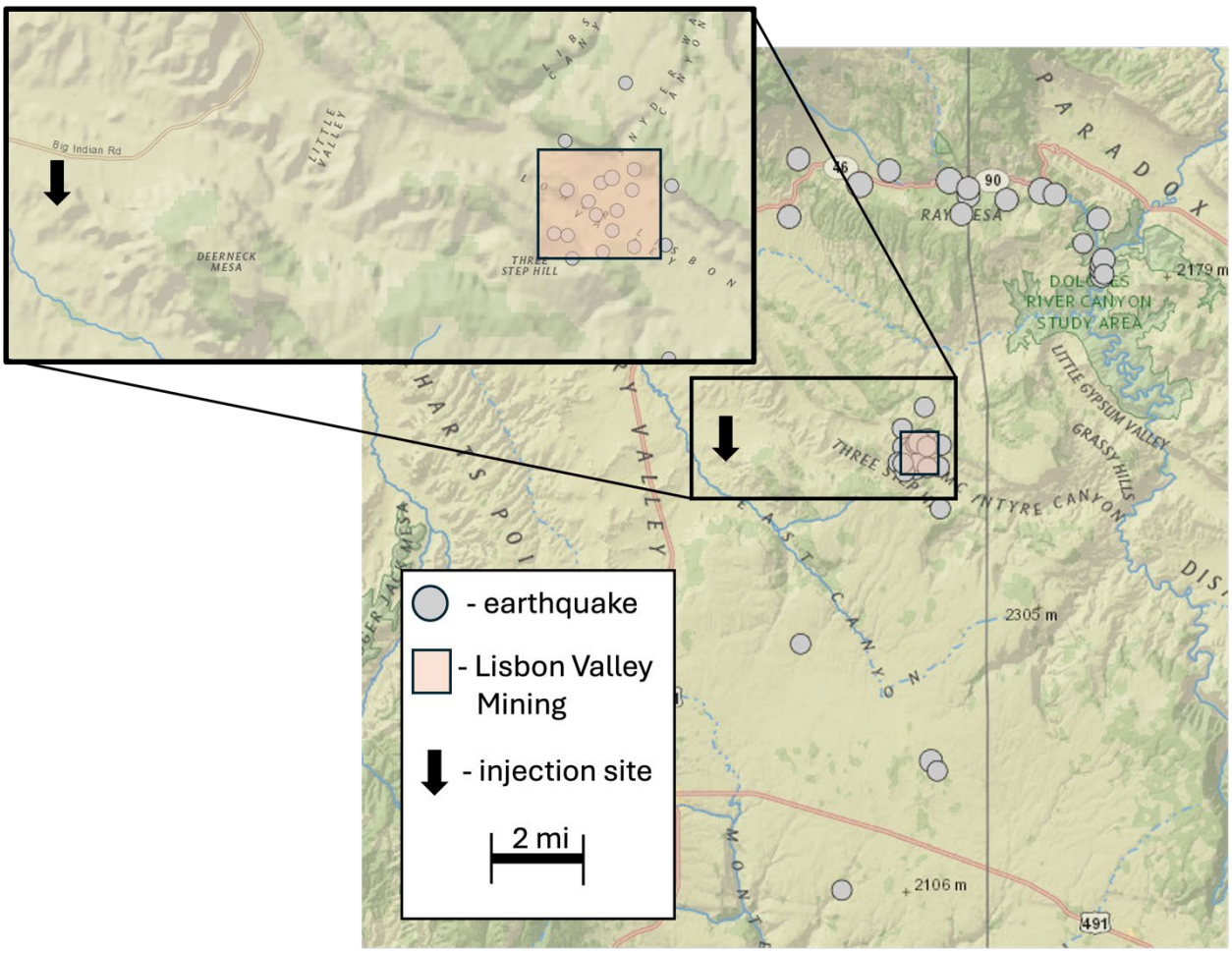

Figure 27: The seismicity recorded in the region surrounding the AGI. Note that the nearest recorded events are most likely mining activities and not earthquakes. A lineament is observed to the north running east-west that might represent a fault zone. Care should be given to make sure no activity is seen between the injection site and the potential fault zone.

Construction of the state of stress

To quantitatively analyze the potential of faults to fail, it is necessary to understand the state of stress in the region. This state of stress is comprised of five components: vertical stress, minimum horizontal stress, maximum horizontal stress, pore pressure, and the direction of the maximum horizontal stress. In some cases, there is data to provide estimates of these parameters, but often assumptions must be made to constrain them. In all cases, reasonable assessments of uncertainty are considered, and Monte Carlo simulations are performed to provide a distribution of the geomechanical stability of the analyzed faults. For this study, we will use the Coulomb failure function (CFF) as the primary metric of geomechanical stability. The CFF is given by,

$$\mathrm{CFF} = |\tau| - \mu\sigma_n, \qquad \text{(Eq. 3)}$$

where τ is the shear stress acting on the fault, μ is the coefficient of friction, and σ_n is the normal stress resolved on the fault. Another key consideration is the depth. We analyze the state of stress at a depth of 8226 ft, which corresponds to the depth of the Leadville, which will be the primary injection target.

Vertical Stress: The best constrained element of the stress state is the vertical stress, which is derived from the integration of density logs. We take a published value of 1.07 psi/ft from a location tens of miles to the northwest, also in the Paradox Basin. For the Monte Carlo simulation, we assume a normal distribution with a standard deviation of 400 psi.

Maximum Horizontal Principal Stress: The maximum horizontal principal stress is derived from the Simpson's coefficient method, which uses regional maps of the relative stress magnitudes or the A_ϕ parameter in conjunction with the assumption that the crust is in frictional faulting equilibrium to arrive at an approximation of stresses with depth. The A_ϕ parameter at the location of the Lisbon site is roughly 1.35, which indicates that the state of stress is in a strike-slip faulting regime – the vertical stress is the intermediate stress. Once the constraint on the maximum horizontal stress is obtained, we use the SoSAT software to obtain reasonable uncertainty on this element of the stress state. For the Monte Carlo simulation, we assume a uniform distribution with a large range of 7000 psi.

Minimum Horizontal Principal Stress: The minimum horizontal principal stress is obtained in the same manner as the maximum. SoSAT is again used to assess uncertainty, and a large range of 5000 psi is assumed with a uniform distribution for the Monte Carlo simulation.

Pore Pressure: We do not possess data on the pore pressure at depth, and thus we assume that the pore pressure is hydrostatic because the sedimentation rate during the deposition of the Leadville was not unusually high. For the Monte Carlo simulation we assume a normal distribution with a standard deviation of 400 psi.

Direction of the Maximum Horizontal Principal Stress: The direction of the maximum horizontal principal stress is taken as N70E from personal correspondence with Professor Dvory, an expert in geomechanics in the Paradox Basin. For the Monte Carlo simulation, we assume a normal distribution with a standard deviate of fifteen degrees.

Coefficient of Friction: The coefficient of friction of laboratory and *in situ* faults tends to be between 0.6 and 0.8. Some authors have shown that a value of 0.6 is reasonable for many materials, so we elect to center a normal distribution on 0.6 with a standard deviation of 0.15 for the Monte Carlo simulations.

Fault Orientations

The Utah Geological Survey identified a set of faults used in the numerical modeling of section 3.2 (Figure 28). The dips of these faults are constrained at roughly 80 degrees. We assume a uniform distribution between 70 and 90 degrees.

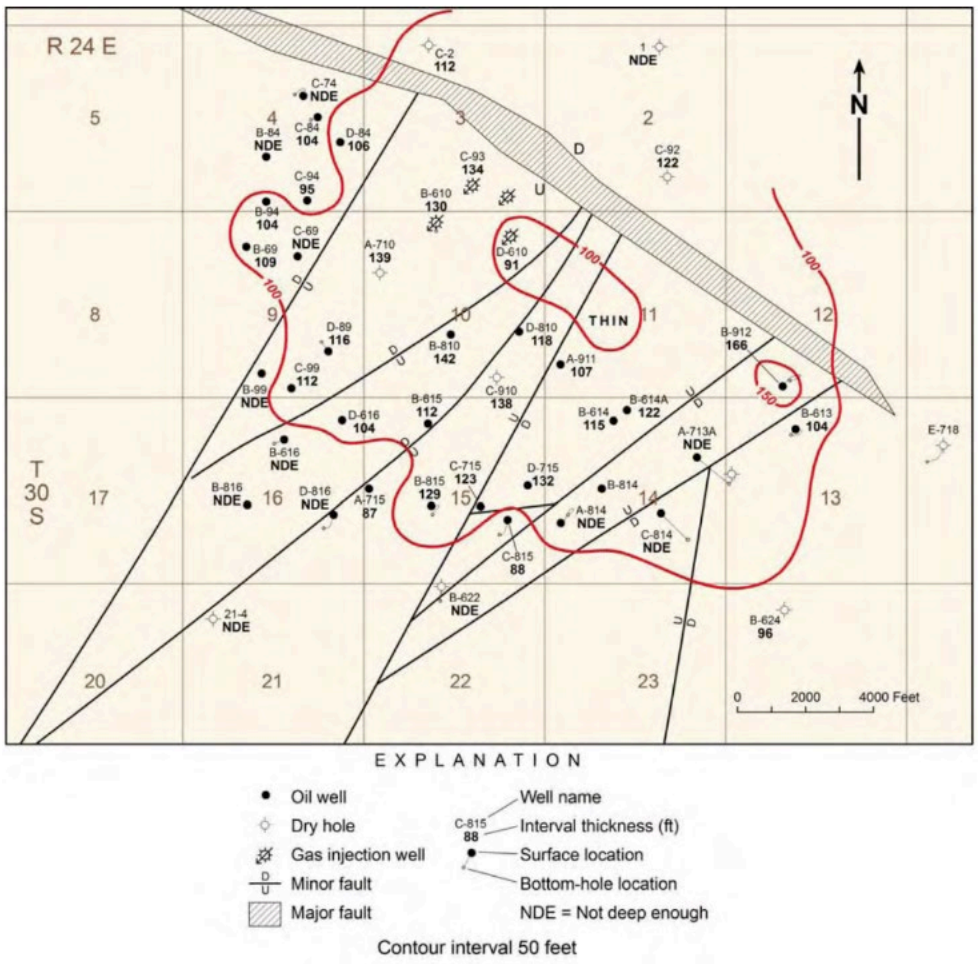

Figure 28: The faults in black obtained by an assessment of the Utah Geological Survey (UGS) on the geology and hydrogeology of the Lisbon Field. The wells are marked as dots, and the red contours correspond to an isochore of a subsection of the reservoir.

The fault orientations are combined with the state of stress in a Monte Carlo manner using 1,000 realizations to acquire the normal and shear stresses that are resolved on the fault. The result is a distribution of the CFFs for each of the three fault orientation groups and each of the five tested dips. These results will be discussed in greater detail below.

Results

The orientations of the faults from the UGS report are shown in Figure 29. These faults are far from the failure equilibrium line (dashed horizontal line), which lends confidence that the injection of the acid gas will not initiate earthquakes along the known faults.

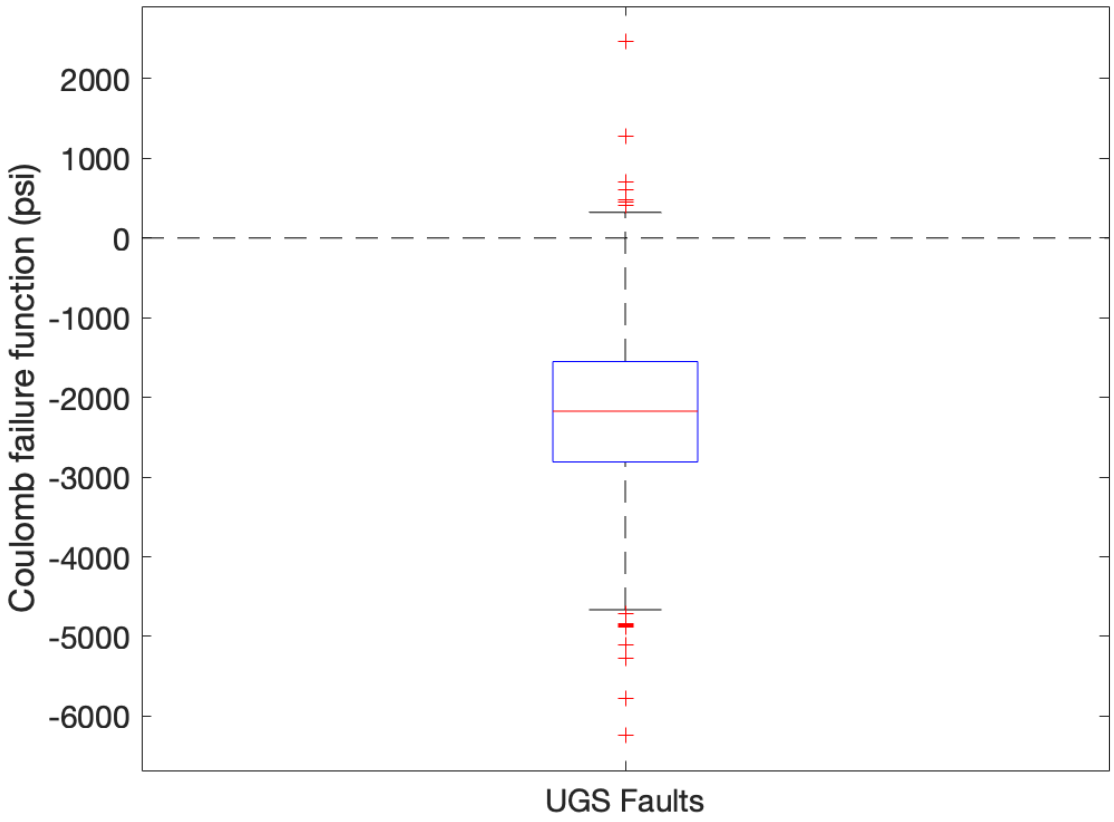

Figure 29: The distribution of CFFs obtained from the Monte Carlo simulation for the Utah Geological Survey fault orientation.

Timing

Leakage due to induced seismicity cannot occur until a damaging event has transpired. In the unlikely event that an earthquake damages the caprock, the leak will persist until the fault surface mineralizes on the order of hundreds of years.

Magnitude

The magnitude of an unlikely leakage scenario is dependent on the magnitude, and more specifically, rupture area of the earthquake. So long as the earthquakes are small, as shown in the past seismicity section, the leakage will likewise be small. Therefore, regional and local monitoring of earthquake activity will provide valuable insight into the quantity of carbon dioxide that might be leaked.

Monitoring

We suggest that the injection of the acid gas will be unlikely to cause rupture on these known faults. The possibility exists for other faults to be present, but we cannot characterize them without data of the fault orientations. The injection appears to be safe with respect to induced seismicity, but we further suggest the installation of a single seismic station using STA/LTA automatic detections conducted by the University of Utah Seismograph Station to monitor and verify that no low-level seismicity is occurring at the site.

5.0 - Detecting and quantifying potential surface leakage of CO_2

Effectively detecting and quantifying undesired leaks of CO_2 from surface infrastructure or natural pathways is a critical component of the MRV plan and is required under 40 CFR § 448(a)(3) Subpart RR. Detecting and quantifying surface leakage requires a multi-point monitoring approach designed to find and mitigate leaks in a timely fashion. These include a distributed controls system (DCS), well testing, H_2S monitors, routine inspections, flux chambers, and water testing.

Distributed Controls System: The first system used for assessing potential leakage is the distributed controls system (DCS) which continuously monitors injection/production rates, pressures, temperature, and composition both in the plant and at active wellheads. The DCS allows engineers and operators to monitor systems in real time and set parameter limit thresholds which trigger an alert to the operator when systems are not functioning as expected. Further investigation into the cause of any triggers will be conducted. These triggers are not necessarily indicative of leakage and the cause can often be quickly identified and resolved by operators without the risk of unwanted leakage.

In cases where the cause of the trigger is not easily identified and resolved, a deeper investigation into the cause of the parameter trigger will be conducted and documented. If a leak is identified, a leakage estimate will be conducted following the leakage quantification section below.

Well Testing: Annual testing of mechanical integrity will be conducted on the Lisbon Unit D-716 well, pursuant of 40 C.F.R. § 146.8. A log of these mechanical integrity tests will be maintained, and testing will be compared against previous/baseline tests to ensure the integrity of the well has not been compromised.

H_2S Monitoring: The CO_2 injection gas is acid gas containing H_2S, a dangerous compound which shall be monitored in real time using various methods to maintain a safe working environment. While dangerous, the presence of H_2S (a volatile compound with extremely low ambient concentrations) provides a useful tracer indicating leakage of the injection gas.

H_2S gas detectors shall be positioned around the facility and will trigger an alarm at ~10ppm. Furthermore, personnel will be equipped with wearable personal H_2S monitors which trigger an alarm at ~5ppm. Because of the high relative concentration of H_2S in the injection gas, leaks from the equipment will trigger an H_2S alarm. An extrusion of H_2S is indicative of leakage of injection gas, and thus an investigation into the cause and remedy for the leak will be conducted in a timely matter.

H_2S sensors are sensitive to small gas extrusions and will be deployed both in both stationary positions as well as on personnel. This allows for both a continuous leakage monitoring system, as well as an effectively mobile system, as personnel wearing sensors will be inspecting equipment and serve as a mobile gas sniffer both in the facility and at well locations.

Routine Inspections: Visual inspections of surface equipment will be conducted on a routine basis. This may include, but is not limited to, inspection of equipment status and integrity, valve positions, proper pressure and flow rates in equipment, and tank volumes. Any faulty equipment detected will be recorded and remedied in a timely manner.

Furthermore, visual and auditory inspections will be conducted routinely, specifically for CO_2 leakage. Cold injected CO_2, if leaked to the atmosphere, typically leads to visible cloud condensation, ice buildup, or audible noise. Inspections will take account of any visible or audible signs of CO_2 leakage and record and remedy them in a timely manner. Following remedy, detected leaks will be quantified using the techniques described in the leakage quantification section below.

Soil-Flux Monitoring: Following the baselining work in the following section, flux values from established collars will be monitored on a seasonal basis for 5 years following the injection period. Measuring soil-flux values seasonally allows growing season trends, which directly impact CO_2 flux from soil, to be adequately considered.

The baselining study will provide threshold values for measured CO_2 flux from collars. Should flux values exceed the defined threshold values, a further investigation into the cause of elevated flux values will be conducted. Often, these exceedance values are a product of natural variability and not indicative of a leak through the soil. As such, more robust investigations should be conducted if specific flux collars exhibit exceedance values for multiple seasons in a row. Flux collars exhibiting persistently high values should be investigated further using the variety of subsurface monitoring and modeling techniques to ensure that leakage through natural pathways has not occurred.

USDW Monitoring: Monitoring USDWs is an important piece of the MRV plan to ensure there is no fugitive extrusion of injected gas into the drinking water supply. At the Lisbon site, the maximum depth of USDW reported by the Utah Division of Water Rights is 1550 ft below ground level at a well site over 7 miles from the Lisbon facility. There exist 6 USDW wells within ½ mile of the Lisbon facility, all of which are less than 300 ft deep. This USDW is therefore much shallower than the injection depth, and there are no reported faults that are connected to these shallow formations.

Despite the low risk of leakage to the USDW, monitoring of the USDW will occur for the duration of the project. An applicable USDW well within the MMA will be selected for monitoring. Temperature, pressure, and fluid composition at this well will be assessed annually for the first 5 years and once every 5 years for the remainder of the monitoring period to ensure no injection gas is leaking into the USDW.

Surface Leakage Quantification: Potential surface leaks of CO_2 are uncertain, and each leakage event can have different causes, natures, and characteristics. There is therefore no one-size-fits-all approach to quantifying CO_2 leaked to the surface during such an event. The nature of the leakage, however, dictates the methodology by which it can be quantified. That is, for leakage concentrated at a well, downhole pressure measurements to inform numerical models will be the most efficient and illustrative. For leakage spread across an areal extent, such as that from confining layer failure, faults, fractures, and seismicity, and lateral migration, the best methods are flux measurements at the surface and again numerical simulations informed from pressure sensors. As such, the most appropriate quantification techniques or combination thereof will be determined on a case-by-case basis.

Leakage estimate will use 40 CFR § 98.230-238 (Subpart W) as a starting point and event-specific engineering estimates (duration, flow rate, component type, etc.) to quantify the mass of CO_2 leaked to the atmosphere.

Determined leakage quantities will be compared with mass balance calculations required in section 7.0 to resolve discrepancies and hone estimates.

6.0 - Determination of Baselines

The surface leakage detection and quantification techniques outlined in section 5.0 define the methods by which potential leaks will be identified. Many of the systems outlined are automated control systems which use target ranges for certain parameter values (pressures, flow rates, gas composition, concentrations, etc.) to alert operators to any unexpected or problematic activity in the system. As such, defining a baseline for these indicator variables is needed to develop the controls and trigger points that will alert operators to potential leakage.

Distributed Controls System (DCS): The DCS will be tuned to effectively monitor and operate systems specific to the Lisbon facility. Target injection rates and pressures will be created according to permitted limits and site-specific modeling results. Operators will program conservative trigger thresholds in the DCS which will identify periods and equipment that may not be operating correctly. Should these thresholds be exceeded, they will be investigated to determine if the alarm has a potential to lead to CO_2 leakage.

Well Testing: Prior to injection, applicable wells will be baselined for various parameters to use as a comparison with annual integrity tests carried out according to section 5.0. These baseline data should include a standard suite of mechanical integrity tests.

H_2S Monitoring: In the absence of fugitive gas emissions, concentrations of H_2S should be traced and not detectable by H_2S sensors deployed stationary or as wearable detectors. The baseline for H_2S excursion and ambient concentration will be assessed at the beginning of the project and is expected to be undetectable due to its low ambient concentration in the atmosphere. Monitoring equipment will be tested with a standard to ensure adequate operation.

Routine Inspections: Baseline routine inspections will be conducted and documented prior to the initiation of injection. These inspections shall be recorded, and work orders generated for any maintenance activity that has potential to lead to CO_2 excursion from the system.

Soil-Flux Monitoring: To evaluate if CO_2 is escaping the reservoir through the soil, an array of flux collars will be deployed and monitored seasonally. Baselining the soil flux should occur prior to the beginning of CO_2 injection. To do so, areas identified as higher risk of natural migration and surface leakage are identified as described in section 4.1. Adequate coverage of the region surrounding the injection wells, as well as potential leakage pathways, will be assessed.

The baselining period for soil flux monitoring should encompass at least four sets of measurements from the collars, one during each season. As CO_2 soil flux is correlated with seasonal trends such as temperature, precipitation, and biological activity, an assessment across seasons is necessary to establish a robust baseline. These measurements will be used to define seasonal flux thresholds using a high percentile of the collected values to account for natural variation. Should flux values collected during and after injection exceed the threshold values, further investigation will be carried out as described in the soil flux section of

task 5.0. Due to natural variation, exceedance of these threshold values is not necessarily indicative of surface leakage. However, should specific flux collars exhibit consistent exceedance values, a more in-depth investigation should be conducted. This may include installing more flux collars near the problem areas, as well as using other monitoring tools to assess the potential for plume migration and natural seepage of CO_2 to the surface.

USDW Monitoring: A water well servicing the USDW above the injection reservoir will be selected to monitor for potential injection gas leakage to the USDW. Upon selection, a baseline for this monitoring well will be established using temperature, pressure, and fluid composition analysis. This baseline will serve as a comparison point for future monitoring efforts in the USDW, and departures from the baseline will be further assessed to confirm no leakage from the injection reservoir has occurred.

7.0 - Determination of Sequestered Mass of CO_2

To comply with § 98.443 [1], the GNG Lisbon Gas Processing Plant will use specific equations to calculate the mass of CO_2 received and sequestered. The calculations include CO_2 received, injected, produced, leaked, and sequestered, using a series of equations designated by the Environmental Protection Agency (EPA) as summarized in Figure 30.

CO_2 Received	CO_2 Sequestered				
Received Equations	**Injection Equations**	**Production/Recycling Equations**	**Surface Leakage Equation**	**Sequestration Equations**	**Equipment Leaks and Vent between Meter and Wellhead**
PR-1 to PR-3	**PR-4 to PR-6**	**PR-7 to PR-9**	**PR-10**	**PR-11**	**Subpart W**

Figure 30: Series of equations to calculate CO_2 received, injected, produced, leaked, and sequestered.

The mass of CO_2 received will be calculated using Equations RR-1 to RR-3. The amount of CO_2 sequestered will be determined using injection equations (RR-4 to RR-6), production/recycling equations (RR-7 to RR-9), surface leakage equations (RR-10), and sequestration equations (RR-12). Additionally, Subpart W [2] provides a calculation procedure for CO_2 emissions resulting from equipment leaks and vented emissions from equipment situated on the surface between the wellheads and the flow meters used to measure injection quantities. Each calculation, as illustrated in Figure 30, is discussed in the following sections with detailed descriptions and equations.

7.1 - Mass of CO_2 Received by Pipeline

The annual mass of CO_2 received by the pipeline at the Lisbon Gas Processing Plant will be calculated using mass or volume flowmeters. The plant has an active carbon capture facility that supplies CO_2 for sequestration as shown in Figure 31.

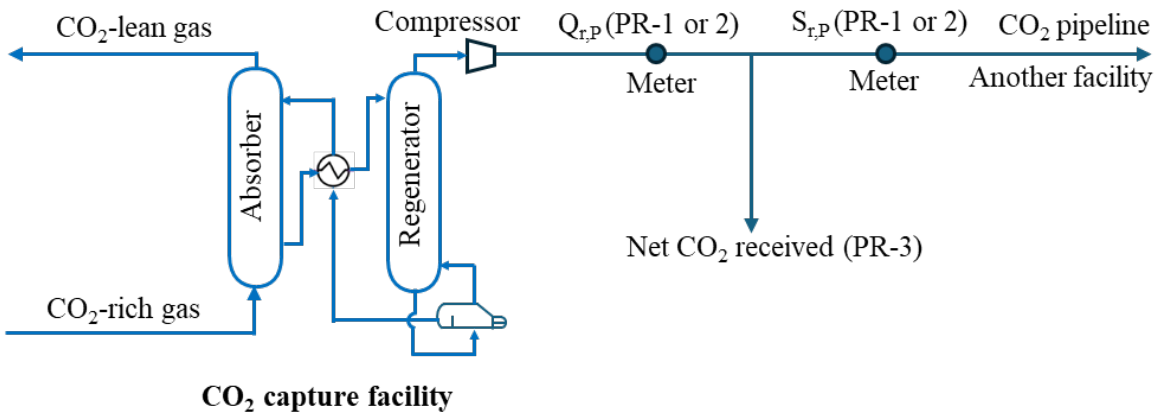

Figure 31: Schematic for Calculating of Mass of CO_2 Received by Pipeline from on-site Carbon Capture Facility.

Furthermore, any CO_2 supplied from other facilities or external sources via pipelines will undergo similar calculations, using the measured volumetric or mass flow rates from the flow meters as depicted in the schematic.

Mass Flow Meter Method

For a mass flow meter, the total annual mass of CO_2 received in metric tons is calculated by multiplying the mass flow by the CO_2 concentration in the flow. Data will be collected quarterly, with mass flow and concentration measurements made in accordance with § 98.444. This is represented by Equation RR-1:

$$CO_{2T,r} = \sum_{p=1}^{4} (Q_{r,p} - S_{r,p}) * C_{CO_{2,p,r}} \qquad \text{(Eq. RR-1)}$$

Where:

- $CO_{2T,r}$ = Net annual mass of CO_2 received through flow meter r (metric tons).
- $Q_{r,p}$ = Quarterly mass flow through a receiving flow meter r in quarter p (metric tons).
- $S_{r,p}$ = Quarterly mass flow through a receiving flow meter r that is redelivered to another facility without being injected into a well in quarter p (metric tons).
- $C_{CO2,p,r}$ = Quarterly CO_2 concentration measurement in flow for flow meter r in quarter p (weight percent CO_2, expressed as a decimal fraction).
- p = Quarter of the year.
- r = Receiving flow meter.

Volumetric Flow Meter Method

For volumetric flow meters, the total annual mass of CO_2 received in metric tons will be calculated by multiplying the volumetric flow at standard conditions by the CO_2 concentration in the flow and the density of CO_2 at standard conditions. Data will be collected quarterly, with volumetric flow and concentration measurements made in accordance with § 98.444. This is represented by Equation RR-2:

$$CO_{2T,r} = \sum_{p=1}^{4} (Q_{r,p} - S_{r,p}) * D * C_{CO_{2,p,r}} \qquad \text{(Eq. RR-2)}$$

Where:

- $CO_{2T,r}$ = Net annual mass of CO_2 received through flow meter r (metric tons).

- $Q_{r,p}$ = Quarterly volumetric flow through a receiving flow meter r in quarter p at standard conditions (standard cubic meters).
- $S_{r,p}$ = Quarterly volumetric flow through a receiving flow meter r that is redelivered to another facility without being injected into a well in quarter p (standard cubic meters).
- D = Density of CO_2 at standard conditions (metric tons per standard cubic meter): 0.0018682.
- $C_{CO2,p,r}$ = Quarterly CO_2 concentration measurement in flow for flow meter r in quarter p (volume percent CO_2, expressed as a decimal fraction).
- p = Quarter of the year.
- r = Receiving flow meter.

Aggregating CO_2 Data Received through Multiple Flow Meters

If CO_2 is received through more than one flow meter, the total mass of all CO_2 received will be summed according to Equation RR-3:

$$CO_2 = \sum_{r=1}^{R} CO_{2T,r} \quad \text{(Eq. RR-3)}$$

Where:

- CO_2 = Total net annual mass of CO_2 received (metric tons).
- $CO_{2T,r}$ = Net annual mass of CO_2 received (metric tons) as calculated in Equation RR-1 or RR-2 for flow meter r.
- r = Receiving flow meter.
- R = Number of receiving flow meters.

7.2 - Mass of CO_2 Injected

The Lisbon Gas Processing Plant will report the annual mass of CO_2 injected according to the procedures specified in paragraphs (c)(1) through (c)(3) of this section.

Mass Flow Meter Method

If a mass flow meter is used to measure the flow of an injected CO_2 stream, the annual mass of CO_2 (in metric tons) injected each year is calculated by multiplying the mass flow by the CO_2 concentration in the flow. This calculation will be done annually, and data will be collected quarterly in accordance with § 98.444. The calculation is performed using Equation RR-4:

$$CO_{2,u} = \sum_{p=1}^{4} Q_{p,u} * C_{CO_{2,p,u}} \quad \text{(Eq. RR-4)}$$

Where:

- $CO_{2,u}$ = Annual CO_2 mass injected (metric tons) as measured by flow meter u.
- $Q_{p,u}$ = Quarterly mass flow rate measurement for flow meter u in quarter p (metric tons per quarter).
- $C_{CO2,p,u}$ = Quarterly CO_2 concentration measurement in flow for flow meter u in quarter p (weight percent CO_2, expressed as a decimal fraction).
- p = Quarter of the year.
- u = Flow meter.

Volumetric Flow Meter Method

If a volumetric flow meter is used to measure the flow of an injected CO_2 stream, the annual mass of CO_2 (in metric tons) injected each year is calculated by multiplying the volumetric flow at standard conditions by the CO_2 concentration in the flow and the density of CO_2 at standard conditions. This calculation will be done annually, and data will be collected quarterly in accordance with § 98.444. The calculation is performed using Equation RR-5:

$$CO_{2,u} = \sum_{p=1}^{4} Q_{p,u} * D * C_{CO_{2,p,u}} \quad \text{(Eq. RR-5)}$$

Where:

- $CO_{2,u}$ = Annual CO_2 mass injected (metric tons) as measured by flow meter u.
- $Q_{p,u}$ = Quarterly volumetric flow rate measurement for flow meter u in quarter p at standard conditions (standard cubic meters per quarter).
- D = Density of CO_2 at standard conditions (0.0018682 metric tons per standard cubic meter).
- $C_{CO2,p,u}$ = Quarterly CO_2 concentration measurement in flow for flow meter u in quarter p (volume percent CO_2, expressed as a decimal fraction).
- p = Quarter of the year.
- u = Flow meter.

Aggregating Injection Data for Multiple Wells

To aggregate injection data for all wells covered under this subpart, the total mass of all CO_2 injected through all injection wells will be summed according to Equation RR-6:

$$CO_{2I} = \sum_{u=1}^{U} CO_{2,u} \quad \text{(Eq. RR-6)}$$

Where:

- CO_{2I} = Total annual CO_2 mass injected (metric tons) through all injection wells.
- $CO_{2,u}$ = Annual CO_2 mass injected (metric tons) as measured by flow meter u.
- u = Flow meter.
- U = Number of receiving flow meters.

7.3 - Mass of CO_2 Produced

There are no fluids currently produced from the Lisbon Valley Field. All of the natural gas processed at the plant comes from fields outside of the MMA. In addition, all of the wells within the MMA have been shut-in or plugged and abandoned (Figures 21 and 22). Furthermore, the only penetration into the Leadville Formation is the injection well, with the total depth of the shut-in wells several layers higher in the White Rim Sandstone. Due to these considerations, it is not feasible that injected CO_2 will be produced back to the surface.

7.4 - Mass of CO_2 Emitted by Surface Leakage

The annual mass of CO_2 emitted by surface leakage will be reported in accordance with the approved MRV plan. The total annual mass of CO_2 emitted from all leakage pathways is calculated using Equation RR-10:

$$CO_{2E} = \sum_{x=1}^{X} CO_{2,x} \quad \text{(Eq. RR-10)}$$

Where:

- CO_{2E} = Total annual CO_2 mass emitted by surface leakage (metric tons) in the reporting year.
- $CO_{2,x}$ = Annual CO_2 mass emitted (metric tons) at leakage pathway x in the reporting year.
- x = Leakage pathway.

Several potential pathways will be considered such as

- Existing wellbores,
- Faults and fractures,
- Natural and induced seismic activity,
- Diffuse leakage through the seal.

7.5 - Net Mass of CO_2 Sequestered in Subsurface Geologic Formations

The Lisbon Gas Processing Plant will report the annual mass of CO_2 sequestered in subsurface geologic formations for the reporting year. A schematic of different components for these calculations is summarized in Figure 32. For the Lisbon Gas Processing Plant, the production comes from other fields.

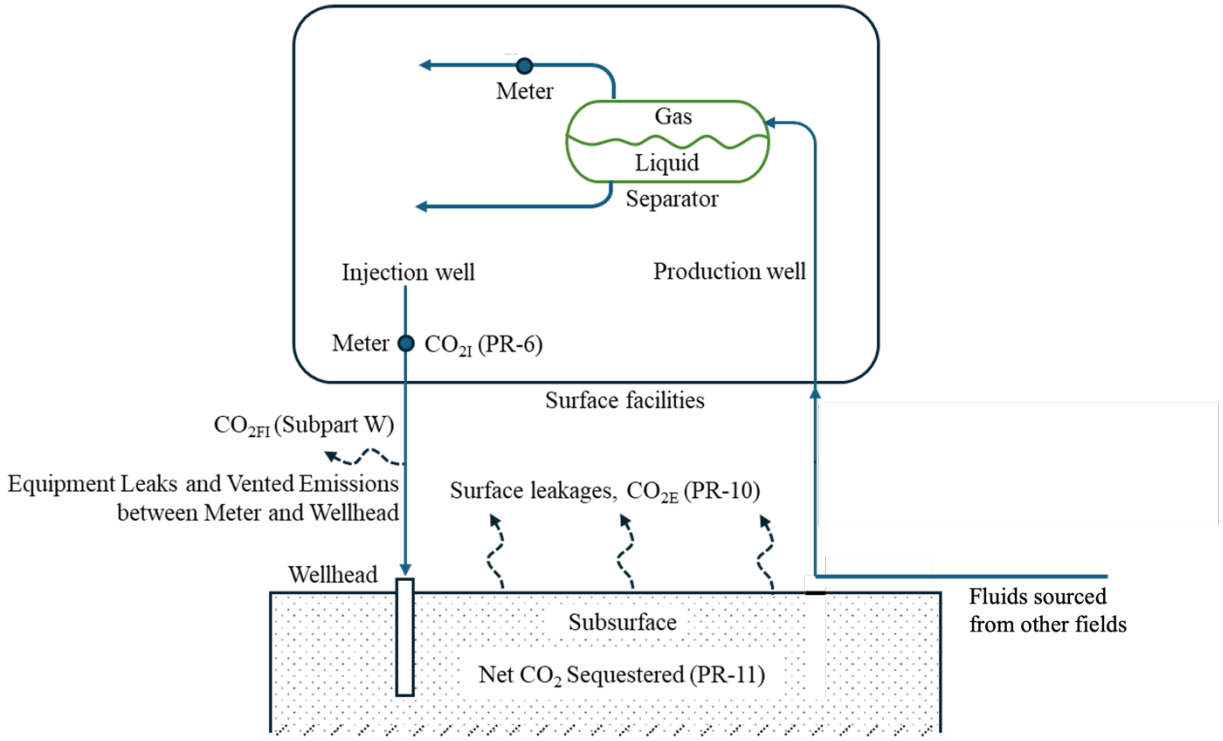

Figure 32: Schematic for Calculating Net Mass of CO_2 Sequestered in Subsurface Geologic Formations.

The annual mass of CO_2 sequestered in the underground subsurface formation will be calculated using Equation RR-12:

$$CO_2 = CO_{2I} - CO_{2E} - CO_{2FI} \qquad \text{(Eq. RR-12)}$$

Where:

- CO_2 = Total annual CO_2 mass sequestered in subsurface geologic formations (metric tons) at the facility in the reporting year.

- CO_{2I} = Total annual CO_2 mass injected (metric tons) in the well or group of wells covered by this source category in the reporting year.
- CO_{2E} = Total annual CO_2 mass emitted (metric tons) by surface leakage in the reporting year.
- CO_{2FI} = Total annual CO_2 mass emitted (metric tons) from equipment leaks and vented emissions of CO_2 from equipment located on the surface between the flow meter used to measure injection quantity and the injection wellhead, for which a calculation procedure is provided in Subpart W [2].

8.0 - Project Schedule

The injection of acid gas into the Leadville Formation began on July 1, 2015, and is projected to continue until the final depletion of the hydrocarbon resources in the Lisbon Valley. The modeling results, calculated for 40 years of active injection, show that the plume will stabilize in roughly 150 years, which will be the end of the monitoring period. This plan will take effect in the second or third quarter of 2025 after proper approval from the EPA.

9.0 - Quality Assurance and Quality Control (QA/QC)

We will comply with the monitoring and QA/QC guidelines outlined in Section 98.444 of Subpart RR, including the requirements of Subpart W for emissions originating from surface equipment, as mandated by Section 98.444(d). There will be four subtasks associated within this task.

9.1 - CO_2 monitoring

In accordance with 40 CFR § 98.3(g)(5)(i), our internal documentation concerning the collection of CO_2 emission data and CO_2 injection data comprises the following:

· Identification of job roles responsible for CO_2 emission data collection and injection data.

· Clarification of the methodologies and processes employed for CO_2 calculations, such as sequestered CO_2 volumes, CO_2 leakage.

· Description of the procedures and methods applied for quality assurance, measurement, maintenance, and repair of all continuous monitoring systems, and other instrumentation used to provide CO_2 data across various stages.

CO_2 Received

CO_2 is received via the pipeline from Lisbon Gas Processing Plant and is measured using a volumetric totalizer, which uses accepted flow calculations for CO_2 according to the AGA Report #3.

CO_2 Injected

The daily CO_2 injection is documented by considering both the recycle compressor meter and the received CO_2 meter from Lisbon, reflecting the 24-hour delivery cycle. This data is taken from the meter daily and archived in our data repositories for records and reservoir management.

CO_2 Produced from plant operations

The gas produced from plant operations is sampled at least once per quarter, immediately upstream or downstream of the flow meter used to measure the flow rate of that CO_2 stream and to measure the CO_2 concentration of the sample. The flow rate of produced CO_2 is measured and collected quarterly.

(1) The point of measurement for the quantity of CO_2 produced from plant operations is a flow meter directly downstream of each separator that sends a stream of gas into a recycle or end-use system.

(2) We will sample the produced gas stream at least once per quarter immediately upstream or downstream of the flow meter used to measure flow rate of that gas stream and measure the CO_2 concentration of the sample.

(3) We will measure the flow rate of gas produced with a flow meter and collect the flow rate quarterly.

CO_2 Emissions from equipment leaks and vented emissions of CO_2

As mandated by 40 CFR § 98.444 (d), we will adhere to the monitoring and QA/QC requirements outlined in Subpart W of the GHGRP for surface equipment positioned between the injection wellhead and the flow meter used for measuring injection quantity, as well as between the production wellhead and the flow meter used for measuring production quantity.

As stipulated by 40 CFR § 98.448 (d) of Subpart RR, we will evaluate leakage from the pertinent surface equipment outlined in Sections 98.233 and 98.234 of Subpart W. According to 40 CFR § 98.233(r)(2) of Subpart W, the emissions factor specified in Table W-1A of Subpart W must be utilized to estimate all gas streams, including the recycle CO_2 stream, for facilities conducting EOR operations. The default emission factors for production equipment are applied to carbon capture utilization and storage injection operations reported under Subpart RR.

9.2 - QA/QC procedures

We will comply with all QA/QC requirements outlined in Subparts A, RR, and W of the GHGRP, as mandated for the development of this MRV plan under Subpart RR. Any measurement devices used to acquire data will be operated and maintained in accordance with relevant industry standards.

9.3 - Estimation of Missing Data

We will estimate any missing data in accordance with the procedures outlined in 40 CFR § 98.445 of Subpart RR of the GHGRP, as mandated. Missing quarterly flow rates of received CO_2 will be estimated using invoices or a representative flow rate value from the nearest previous period. Similarly, missing quarterly CO_2 concentrations of received streams will be estimated using invoices or a representative concentration value from the nearest previous period.

If a quarterly quantity of injected CO_2 is missing, it will be estimated using a representative quantity injected from the nearest previous period at a similar injection pressure. For any values associated with CO_2 emissions from equipment leaks and vented emissions of CO_2 from surface equipment at the facility

reported in this subpart, missing data estimation procedures specified in Subpart W of 40 CFR Part 98 will be followed. If the quarterly quantity of CO_2 produced from subsurface geologic formations is missing, it will be estimated using a representative quantity produced from the nearest previous period.

9.4 - Revisions of the MRV plan

We will revise the MRV plan as necessary to accommodate changes in production processes, monitoring instrumentation, and quality assurance procedures. Additionally, we will enhance procedures for the maintenance and repair of monitoring systems to minimize equipment downtime.

10.0 - Records Retention

GNG Energy will follow the record retention requirements of 40 CFR § 98.3(g). In addition, it will carefully collect, generate, and aggregate records for:

- Quarterly records of CO_2 generated by the Lisbon Gas Processing Plant, including temperature and pressure as well as concentration.
- Quarterly records of injected CO_2, including volumetric flow at standard conditions and operating conditions, temperature and pressure, and concentration.
- Annual records of information used to calculate the CO_2 emitted from surface and subsurface leakage pathways.

11.0 - References

G. A. Bradley, "Lisbon Field, Utah," *Four Corners Geological Society Guidebook,* vol. 8th Field Conference, 1975.

Blakey RC (1990) Stratigraphy and geologic history of Pennsylvanian and Permian rocks, Mogollon Rim region, central Arizona and vicinity. GSA Bull 102:1189–1217. https://doi.org/10.1130/0016-7606(1990)102<1189:SAGHOP>2.3.CO;2

Blakey RC, Havholm KG, Jones LS (1996) Stratigraphic analysis of eolian interactions with marine and fluvial deposits, Middle Jurassic Page Sandstone and Carmel Formation, Colorado Plateau, U.S.A. J Sediment Res 66:324–342. https://doi.org/10.1306/D426833D-2B26-11D7-8648000102C1865D

Chidsey, T. (2008). *The Mississippian Leadville Limestone exploration play, Utah and Colorado-exploration techniques and studies for independents*. State Of Utah (United States). Funding organization: US Department of Energy.

Department of Natural Resources, Utah Division of Oil, Gas, and Mining, "Summary Production Report by Field," Utah Division of Oil, Gas, and Mining, Salt Lake City, 2024.

Gasda, Sarah E., Stefan Bachu, and Michael A. Celia. 2004. Spatial characterization of the location of potentially leaky wells penetrating a deep saline aquifer in a mature sedimentary basin. Environmental geology, 46, pp. 707-720.

Goral J, Panja P, Deo M, et al. Confinement effect on porosity and permeability of shales[J]. Scientific reports, 2020, 10(1): 49.

Hite RJ, Buckner DH (1981) Stratigraphic correlations, facies concepts, and cyclicity in Pennsylvanian rocks of the Paradox Basin. Rocky Mt Assoc Geol 1981 Field:147–159

Kirkland JI, Suarez M, Suarez C, Hunt-Foster R (2016) The Lower Cretaceous in east-central Utah—The Cedar Mountain Formation and its bounding strata. Geol Intermt West J Utah Geol Assoc 3:101–228. https://doi.org/10.31711/giw.v3i0.9

Lackey, G., Vasylkivska, V.S., Huerta, N.J., King, S. and Dilmore, R.M. 2019. Managing well leakage risks at a geologic carbon storage site with many wells. International Journal of Greenhouse Gas Control, 88, pp. 182–194.

Leake SA, Hoffmann JP, Dickinson JE (2005) Numerical ground-water change model of the C aquifer and effects of ground-water withdrawals on stream depletion in selected reaches of Clear Creek, Chevelon Creek, and the Little Colorado River, northeastern Arizona

Lessentine RH (1965) Kaiparowits and Black Mesa Basins: Stratigraphic Synthesis1. Am Assoc Pet Geol Bull 49:1997–2019. https://doi.org/10.1306/A663387E-16C0-11D7-8645000102C1865D

M. L. Matheny, "A History of the Petroleum Industry in the Four Corners," *Oil and Gas Fields of the Four Corners,* Vols. I-II, pp. 17-24, 1978.

Mcpherson ML, Currie BS, Pierson JS, Survey UG (2006) Reservoir Characterization of the Cretaceous Cedar Mountain and Dakota Formations, Southern Uinta Basin: Year-One Report Open-File Report 492
Morgan CD (2015) Understanding Southeast Utah's Cane Creek Oil, a Continuing Challenge. Surv Notes Utah Geol Surv 47:

NRAP-open-IAM: A flexible open-source integrated-assessment-model for geologic carbon storage risk assessment and management. Environmental Modelling & Software, 143, p. 105114.

National Risk Assessment Partnership (NRAP). 2023. Overview of NRAP-OPEN-IAM. https://gitlab.com/NRAP/OpenIAM.

Rasmussen L, Rasmussen D. (2009) Burial history analysis of the Pennsylvanian petroleum system in the deep Paradox Basin Fold and Fault Belt, Colorado and Utah. In: Houston WS, Wray LL, Moreland PG (eds) The Paradox Basin revisited : new developments in petroleum systems and basin analysis, RMAG Speci. Rocky Mountain Association of Geologists, Denver

Repenning CA, Page HG (1956) Late Cretaceous Stratigraphy of Black Mesa, Navajo and Hopi Indian Reservations, Arizona1. Am Assoc Pet Geol Bull 40:255–294. https://doi.org/10.1306/5CEAE31F-16BB-11D7-8645000102C1865D

Rice CA (2003) Production waters associated with the Ferron coalbed methane fields, central Utah: chemical and isotopic composition and volumes. Int J Coal Geol 56:141–169. https://doi.org/10.1016/S0166-5162(03)00086-7

D. M. Seneshen, T. C. Chidsey, C. D. Morgan and M. D. Vanden Berg, "New Techniques for New Hydrocarbon Discoveries-Surface Geochemical Surveys in the Lisbon and Lightning Dray Southeast Field Areas, San Juan County, Utah," Utah Department of Natural Resources, Salt Lake City, 2010.

G. Sheehan, Notice of Intent to Prepare an Environmental Impact Statement for the Proposed Lisbon Valley Mining Company, LLC Copper Mine Plan of Operations Modification, San Juan County, Utah, 103 ed., vol. 89, 2024, pp. 46,155-46,157.

Shi R, Liu J, Wang X, et al. A critical analysis of shale laboratory permeability evolution data[J]. Energy, 2021, 236: 121405.

Trudgill BD (2011) Evolution of salt structures in the northern Paradox Basin: Controls on evaporite deposition, salt wall growth and supra-salt stratigraphic architecture. Basin Res 23:208–238. https://doi.org/10.1111/J.1365-2117.2010.00478.X

Vasylkivska, V., Dilmore, R., Lackey, G., Zhang, Y., King, S., Bacon, D., Chen, B., Mansoor, K. and Harp, D. 2021.

Whidden KJ, Lillis PG, Anna LO, et al (2014) Geology and total petroleum systems of the Paradox Basin, Utah, Colorado, New Mexico, and Arizona. Mt Geol 51:119–139